CONFIDENTIAL

Copy 284
RM E50H10

NACA RM E50H10

NACA

RESEARCH MEMORANDUM

DOWNWASH IN VORTEX REGION BEHIND RECTANGULAR HALF-WING AT MACH NUMBER 1.91

By John L. Cummings and Rudolph C. Haefeli

Lewis Flight Propulsion Laboratory
Cleveland, Ohio

NATIONAL ADVISORY COMMITTEE
FOR AERONAUTICS

WASHINGTON
October 26, 1950

CONFIDENTIAL

NATIONAL ADVISORY COMMITTEE FOR AERONAUTICS

RESEARCH MEMORANDUM

DOWNWASH IN VORTEX REGION BEHIND RECTANGULAR HALF-WING AT MACH NUMBER 1.91

By John L. Cummings and Rudolph C. Haefeli

SUMMARY

The results of an experimental investigation to determine the downwash in the region of the trailing vortex system behind a rectangular half-wing in a supersonic stream are presented. The half-wing had an aspect ratio of 1.667, a 5-percent-thick symmetrical diamond cross section, and was beveled to a knife edge at the tip. The investigation was made at a Mach number of 1.91 and a Reynolds number of 1.56×10^6 based on the wing chord. A wake survey was also conducted.

At small angles of attack, the experimental spanwise variation of $-d\epsilon/d\alpha$ (where ϵ is the downwash angle and α is the angle of attack) generally followed the trends indicated by linearized theory based on the assumption that the trailing vortex sheet was undistorted. At higher angles of attack, the downwash field was greatly influenced by the rolling up of the vortex sheet. At each chordwise station the downwash field progressively changed with increasing angle of attack from that induced by an undistorted vortex sheet toward that induced by a completely rolled-up vortex sheet. The form and the location of the vortex sheet was indicated by a wake survey.

INTRODUCTION

The rational design of an aircraft empennage is dependent on the knowledge of the downwash field behind the wing. Several theoretical methods based on linearized flow exist for computing the downwash behind wings in a supersonic stream (for example, references 1 to 3). Experimental investigations are still required, however, to verify the theoretical results and to provide bases for refining the theory.

Investigations of the downwash behind rectangular wings at Mach numbers of 1.53 and 2.41 are reported in references 4 and 5. In these investigations, the experimental trends of the variation of the downwash angle with angle of attack at zero lift were generally found to be similar to those predicted by linearized theory. The displacement and distortion of the trailing vortex sheet were found to affect the downwash at angle of attack.

It has been apparent that a knowledge of the location and strength of the trailing vortex sheet is required to explain experimental deviations from the predictions of linearized theory. Methods for calculating the distortion of the trailing vortex sheet and its effect on the downwash are discussed in reference 6. Comparisons between theory and experiment of the distortion of the trailing vortex sheet and its effect on the downwash at supersonic flight speeds, however, remain scarce.

For a more thorough knowledge of the characteristics of the trailing vortex sheet, the downwash in the vicinity of the wake has been investigated in an experimental program at the NACA Lewis laboratory. The first part of this investigation is reported in reference 7, wherein theoretical and experimental values of the downwash in the wake region of a trapezoidal wing at a Mach number of 1.91 are compared. Experimental deviations from the linearized downwash values are attributed to differences between the theoretical and actual spanwise distributions of shed vorticity and to the distortion of the vortex sheet in the form of a rotation about the center of the theoretical vortex sheet. The second part of the investigation, concerning the downwash behind the tip region of a rectangular wing at a Mach number of 1.91, is discussed herein.

APPARATUS

The downwash investigation was conducted in the NACA Lewis 18- by 18-inch supersonic wind tunnel. The free-stream Mach number in the region of the wing and of the downwash survey was 1.91 $\pm$0.01. The Reynolds number was 1.56×10^6 based on the wing chord.

The model was a rectangular half-wing (fig. 1) with a 5-percent-thick symmetrical diamond cross section, a 10-inch semispan, and a 6-inch chord. The wing, machined from SAE 4140 steel, had finished surfaces ground to 16 microinches and knife edges at the leading, trailing, and side edges. The wing was mounted on the tunnel wall and could be pivoted about the midpoint of the root chord.

Five wedges with static-pressure orifices on each face (figs. 2 and 3(a)), mounted with centers 7/8 inch apart, were used to measure the downwash angles. The support system and mechanism for changing wedge angle of attack (figs. 1 and 3(a)) described in reference 7 were also used, although the support system was slightly modified to allow the wedge position to be changed in 7/16-inch increments in the spanwise (y) direction. Five tetrabromoethane U-tube manometers, one connected to each wedge, were used to obtain the static-pressure differential of the wedges.

The 41-tube pitot-pressure rake described in reference 7 was used for the wake survey (fig. 3(b)).

In an auxiliary investigation, a flat plate was mounted perpendicular to the air stream to generate a strong shock wave behind the wing tip (fig. 3(c)).

PROCEDURE

In a previous investigation reported in reference 7, downwash angles were determined using a null method; that is, the static pressures on opposite sides of a wedge placed in the downwash field were balanced and the inclination of the wedge was then measured. This method established the direction of the air stream at the wedge apex. Inasmuch as excessive time was required to balance the static pressures, a faster method of determining the flow angle was developed for the present experiment.

In this investigation, the flow angle was determined by taking two readings of wedge inclination (within 1.5° of the actual flow angle) and the corresponding static-pressure differentials across the wedge. The wedge inclination corresponding to zero static-pressure differential was then found by a linear interpolation. The interpolation for the inclination corresponding to zero static-pressure differential across the wedge was justified by a wedge calibration which indicated that the static-pressure differential is proportional to wedge angles of attack for angles less than 1.5°.

The downwash angle at any station was assumed to be the difference between the flow angle obtained with the wing at an angle of attack and the flow angle obtained with the wing at an angle of attack of 0°. Downwash angles were determined for a range of wing angles of attack between -8° and 8° for the stations indicated in figure 4. Chordwise stations are designated by their distance in chords behind the wing leading edge. Coordinates of spanwise stations are presented in table I. The symbols used herein are defined in appendix A.

The wake survey was conducted at the stations indicated in figure 4 for wing angles of attack of 0°, -4°, and -8°.

Schlieren photographs were taken with a flat plate mounted behind the wing trailing edge to obtain an estimate of the spanwise position of the minimum total pressure in the wake.

THEORY

The perturbation velocities behind a wing are dependent on the strength and the location of the shed vorticity. Vorticity is shed in the form of a vortex sheet from the trailing edge of a lifting surface with a spanwise load gradient. Generally, this vortex sheet rolls up at its outboard edges until the entire vorticity is ultimately concentrated in two cores that trail behind the wing tips at the vortex centers of gravity (reference 6).

The vortex sheet rolls up faster when the wing is at larger angles of attack inasmuch as the perturbation velocities (downwash and sidewash), which in effect cause the distortion, increase with angle of attack. Simultaneously with the rolling up at the edges, the remainder of the vortex sheet is displaced downward by the vertical perturbation velocities (downwash). For the rectangular wing, the distance behind the trailing edge at which the trailing vortex sheet may be considered essentially rolled up is (by the method of reference 6)

$$\frac{e'}{c} = 1.5 \frac{s'^2}{C_L S'} \frac{s'}{c} \tag{1}$$

where s' and S' are the span and area, respectively, of the tip region $\left(-1 \leqq \frac{\beta y'}{c} \leqq 0\right)$ of the half wing.

The method of reference 8 was used to obtain a theoretical estimate of the form and the location of the distorted vortex sheet. In this method, the trailing vortex sheet is represented by a finite number of trailing line vortices. The displacement of each line vortex (caused by the sidewash and downwash induced by the remaining line vortices) during successive time intervals is calculated. The displacements of all the line vortices then define the distortion of the shed vortex sheet. Using the lifting line approximation discussed in appendix B, the method for calculating the distortion is developed in appendix C.

Theoretical values of the downwash parameter $-d\epsilon/d\alpha$ behind the rectangular wing were computed assuming that the trailing vortex sheet is (1) undistorted or (2) completely rolled up. The actual downwash field progressively changes from that induced by the undistorted vortex sheet to that induced by the completely rolled up vortex sheet as the angle of attack or the downstream distance is increased. Lifting line methods (references 1 and 9) were used to determine the downwash parameter $-d\epsilon/d\alpha$ for the case where the vortex sheet is assumed to be undistorted and to lie in the plane of the wing (z=0 plane). The equations are presented in appendix B. The charts of reference 2 were employed to determine values of $-d\epsilon/d\alpha$ at stations near the Mach cone from the leading edge where lifting line theory yields inaccurate results. A single line vortex with circulation Γ_m, located (in the z=0 plane) spanwise at the center of gravity of the undistorted vortex sheet behind the half-wing, was used to represent the completely rolled up vortex sheet. For the experimental wing (fig. 4), the spanwise location of the vortex center of gravity is

$$\bar{y} = \int_{-1}^{0} \frac{\Gamma(y_0)}{\Gamma_m} dy_0 = -0.252$$

RESULTS AND DISCUSSION

Wake Survey

The wake profiles for angles of attack of 0°, 4°, and 8° are presented for each station in figure 5. The wake intensity $\Delta H/H$ is plotted as a function of z. At all spanwise stations the wake widens and has a lower maximum intensity with increasing distance downstream. In the region near $y = \frac{\beta y'}{c} = 0$, a comparatively large increase in maximum wake intensity and wake width occurs at the higher angles of attack (fig. 5(c)). In this region also, the curves generally exhibit two maximums (at spanwise stations m, n, and l in figs. 5(b) and 5(c)). The upper, broader maximum is the result of the rolling up of the vortex sheet. The breadth of the curve associated with this maximum indicates the extent of the core of vorticity. (The term core of vorticity denotes the rolled up parts of either a partly rolled up or a fully rolled up vortex sheet.) The lower maximum locates the relatively undistorted part of the vortex sheet.

The vertical coordinates of the wake intensity maximums are plotted for an angle of attack of 8° at the 1.5-chord station (x = 1.5) and the 3-chord station (x = 3.0) in figure 6. These maximums define the location of the trailing vorticity (reference 10). The theoretical displacement of the vortex sheet (as determined from equation (C4) using 10 equally spaced line vortices with n = 2/5) is presented for comparison. Theoretical vortex sheet displacements near the tip are not indicated inasmuch as the vortex spiral in this region is not accurately defined by these equations. The region of the wake survey (fig. 5) that has a pressure deficiency, and which therefore indicates the spread of the wake directly behind the wing, is indicated by slant lines. These lines are dashed where the extent of the wake is less clearly defined by the wake survey. The progressive rolling up of the vortex sheet is indicated by the growth, with increase in x, of the large shaded region near y = 0.

The discrepancies between the theoretical and experimental locations of the shed vorticity result from the simplifying assumptions of the theory. The present method, however, gives better agreement with the experimental results of this investigation than the method (described in reference 4) of integrating the downwash angle with respect to distance along a streamline. It is evident that a more accurate theoretical determination of the vortex sheet location is desirable.

Downwash Survey

Theoretical and experimental variations of downwash angle with angle of attack are compared in figure 7. The theoretical values, based on the assumption of an undistorted vortex sheet, were obtained either from lifting line theory (equation (B1)) or from the charts of reference 2. In general, at each station the experimental points form a smooth symmetrical curve about the coordinate origin. The nonlinearity of these curves is mainly the result of the displacement and the rolling up of the trailing vortex sheet as the downstream distance or the angle of attack is increased.

Experimental spanwise variations of $-d\epsilon/d\alpha$ are compared in figure 8 with theoretical variations for each chordwise station. Data for plotting experimental points were obtained by measuring the slope of the curves in figure 7 at angles of attack of 0°, 4°, and 7°. Faired experimental curves are included for the 3-chord station in the plane of the wing (x=3, z=0, fig. 8(a)) to show significant trends. Two theoretical curves of the spanwise variation of $-d\epsilon/d\alpha$ based on the limiting assumptions of an undistorted vortex

sheet and of a completely rolled up vortex sheet are included for comparison. The completely rolled up vortex sheet for the rectangular half-wing is represented by a single line vortex located (in the z=0 plane) spanwise at the vortex center of gravity $\bar{y} = \frac{\overline{\beta y'}}{c} = -0.252$.

At the x = 3, z = 0 station (fig. 8(a)), the experimental values of $-d\epsilon/d\alpha$ for an angle of attack of 0° are in close agreement with the theory based on the assumption of an undistorted vortex sheet. As the angle of attack is increased to 4°, and then to 7°, however, the experimental curves approach the curve produced by the single line vortex. This trend is a direct result of the rolling up of the vortex sheet. Theoretically, the rolling up process is almost complete at the x = 3 station for $\alpha = 7^\circ$, inasmuch as the rolling up distance is then $(e'+c)/c = 3.52$ (from equation (1)). The trends of the experimental curves indicate that the center of the core of vorticity is located near y = -0.12 for $\alpha = 4^\circ$ and near y = -0.16 for $\alpha = 7^\circ$.

For the x = 3, z = 0.353 station (fig. 8(b)), the comparatively large negative values of $-d\epsilon/d\alpha$ near y = -0.2 for $\alpha = 4^\circ$ and near y = -0.4 for $\alpha = 7^\circ$ indicate that the center of the core of vorticity is in effect closer to the experimental stations than the theoretical line vortex (assumed to lie in the z=0 plane). At an angle of attack of -4°, by chance, the effects of the core of vorticity and the displaced vortex sheet combine to produce the result theoretically predicted with the assumption of an undistorted vortex sheet. At this angle of attack the survey stations are closer to the unrolled part of the vortex sheet than to the center of the core of vorticity.

At the 1.5-chord station (x=1.5, z=0), the vortex sheet is less distorted than at the 3-chord station (fig. 6). At x = 1.5, the experimental values of $-d\epsilon/d\alpha$ for 4° and 7° angles of attack (fig. 8(c)) therefore lie closer to the theoretical values based on the assumption of an undistorted vortex sheet than those at x = 3 (fig. 8(a)). The strength of the core is considerably less than that indicated at the 3-chord station. The trends of the experimental points at x = 1.5 (fig. 8(c)) indicate that the center of the core of vorticity is located near y = -0.04 for $\alpha = 4^\circ$ and near y = -0.10 for $\alpha = 7^\circ$.

The experimental data of figure 8 thus indicate the rate of rolling up of the vortex sheet with downstream distance and angle of attack. The approximate location of the center of the core of vorticity moves inboard toward the theoretical value of $\bar{y}$ as the vortex sheet rolls up.

Auxiliary Survey of Tip Region of Wake

Typical flash schlieren photographs taken with a flat plate installed downstream of the wing (fig. 3(c)) are shown in figure 9 for wing angles of attack of -2° and -8°. At angle of attack, the bow wave caused by the flat plate is preceded by a conical shock that occurs because of the decrement in total pressure downstream of the wing side edge (indicated in fig. 5). As the angle of attack is increased, the total pressure behind the wing side edge decreases and the conical shock occurs farther upstream. The apex of the conical shock is believed to occur at the location of the pitot-pressure minimum (the wake survey is not extensive enough to verify this) and to indicate the position of the trailing vortex core in regions where the trailing vortex sheet has begun to roll up. The technique of artificially introducing a strong shock behind a supersonic wing to detect the presence and the location of trailing vortex cores was suggested by Harold Mirels of the NACA Lewis laboratory.

This investigation indicates that the usual detached shock configuration ahead of an obstacle in a supersonic stream is greatly modified by the presence of a wake. Thus, for example, flow measurements with instruments having relatively blunt leading edges require correction for the abnormal shock configuration in the vicinity of the wake region.

The conical shock angle (fig. 9(b)) closely agrees with the theoretical shock angle obtained for a cone with an apex angle equal to the angle formed by the lines bounding the subsonic region within the experimental conical shock (omitting the region of large curvature near the apex). The subsonic region is therefore probably a region of approximately constant static pressure in which low eddying velocities exist.

CONCLUDING REMARKS

The results of an investigation of the downwash and wake in the region of the trailing vortex sheet behind a rectangular half-wing at a Mach number of 1.91 have been presented.

At small angles of attack, the experimental spanwise variation of $-d\epsilon/d\alpha$ generally follows the trends indicated by linearized theory based on the assumption that the trailing vortex sheet is undistorted. At higher angles of attack, however, the downwash field in the vicinity of the vortex sheet is greatly influenced by the rolling up of the vortex sheet. The form and the location of the vortex sheet is indicated by the wake survey.

The large influence of vortex sheet distortion on the downwash in the vicinity of the vortex sheet emphasizes the need for a comprehensive experimental program to verify and extend existing theory for the rolling up of the vortex sheet and its effect on the downwash field.

Lewis Flight Propulsion Laboratory,
National Advisory Committee for Aeronautics,
Cleveland, Ohio.

APPENDIX A

SYMBOLS

The following symbols are used in this report:

C_L lift coefficient of tip region ($-1 \leqq y \leqq 0$) of half wing, $\frac{L}{\frac{\rho}{2} U^2 S'}$

c wing chord (0.5 ft on model)

e' distance downstream of wing trailing edge at which trailing vortex sheet is essentially rolled up

H pitot pressure in free stream

H_w pitot pressure in wake

ΔH $H-H_w$

L lift of wing

M free-stream Mach number

n defined in appendix C

$r_i = \sqrt{(x-x_1)^2-(y-y_i)^2-(z-z_1)^2}$

$r_0 = \sqrt{(x-x_1)^2-(y-y_0)^2-(z-z_1)^2}$

S' area of tip region ($-1 \leqq y \leqq 0$) of half wing

s' span of tip region ($-1 \leqq y \leqq 0$) of half wing

U free-stream velocity

u, v, w perturbation velocity components in x',y',z' directions, respectively

$x = \frac{x'}{c}$

$y = \frac{\beta y'}{c}$

$z = \frac{\beta z'}{c}$

$\bar{y}$ spanwise coordinate of center of gravity of vortex system

x', y', z' Cartesian coordinate system with origin at outboard tip of leading edge of wing at 0° angle of attack (fig. 4); x' axis is in free-stream direction

α angle of attack

β cotangent of Mach angle, $\sqrt{M^2-1}$

Γ circulation of wing

Γ_m circulation at midspan of complete wing

ϵ downwash angle (positive in negative z-direction)

ρ free-stream density

Subscripts:

0 integration variable

1 location of lifting line

i coordinates of trailing line vortices

APPENDIX B

EQUATIONS FOR LIFTING-LINE APPROXIMATION

For an unbent lifting line (horseshoe-vortex system) lying along the line x_1, z_1, the downwash parameter at a station x,y,z is given by (reference 1)

$$\frac{d\epsilon}{d\alpha} = \frac{\beta}{2\pi c\alpha U}\int_{y_a}^{y_b} \frac{(x-x_1)(y-y_0)\left[r_0^2-(z-z_1)^2\right]}{r_0\left[(x-x_1)^2-(z-z_1)^2\right]\left[(y-y_0)^2+(z-z_1)^2\right]} \frac{d\Gamma}{dy_0}\, dy_0 \qquad (B1)$$

where y_a and y_b are the ordinate limits of the lifting line contained within the forward Mach cone from the point x,y,z. A nondimensional coordinate system is so employed that

$$\left.\begin{aligned} x &= \frac{x'}{c} \\ y &= \frac{\beta y'}{c} \\ z &= \frac{\beta z'}{c} \end{aligned}\right\} \qquad (B2)$$

where x', y', and z' are the physical coordinates with origin defined in the list of symbols.

For a semi-infinite rectangular wing the circulation Γ, evaluated along the trailing edge, is constant $\left(\Gamma = \frac{4c\alpha U}{\pi\beta}\right)$ except in the tip region $(-1 \leq y \leq 0)$ where

$$\Gamma = \frac{4c\alpha U}{\pi\beta}\left[\sqrt{-y(1+y)} + \tan^{-1}\sqrt{\frac{-y}{1+y}}\right] \qquad (B3)$$

and the shed vorticity is

$$\frac{d\Gamma}{dy} = \frac{-4c\alpha U}{\pi\beta}\sqrt{\frac{1+y}{-y}} \qquad (B4)$$

The spanwise distribution of Γ and $d\Gamma/dy$ for a rectangular wing is presented in figure 10.

APPENDIX C

DISTORTION OF TRAILING-VORTEX SHEET

An unbent lifting line may be approximated by a finite number of horseshoe vortices (reference 10). The downwash induced by these horseshoe vortices is, from equation (B1),

$$w = -\frac{\beta\Gamma_m}{2\pi c}\sum_i \frac{(x-x_1)(y-y_i)\left[(x-x_1)^2-(y-y_i)^2-2(z-z_i)^2\right]}{r_i\left[(x-x_1)^2-(z-z_i)^2\right]\left[(y-y_i)^2+(z-z_i)^2\right]}\left(\frac{\Delta\Gamma}{\Gamma_m}\right)_i \qquad (C1)$$

Similarly, the downwash induced by a system of trailing line vortices is (reference 1)

$$w = -\frac{\beta\Gamma_m}{2\pi c}\sum_i \frac{(x-x_1)(y-y_i)}{r_i\left[(y-y_i)^2+(z-z_i)^2\right]}\left(\frac{\Delta\Gamma}{\Gamma_m}\right)_i \qquad (C2)$$

Inasmuch as the bound vortices do not contribute to the sidewash, the sidewash may be obtained from equation (C2) by replacing $(y-y_i)$ with $-(z-z_i)$ in the numerator. Thus,

$$v = \frac{\beta\Gamma_m}{2\pi c}\sum_i \frac{(x-x_1)(z-z_i)}{r_i\left[(y-y_i)^2+(z-z_i)^2\right]}\left(\frac{\Delta\Gamma}{\Gamma_m}\right)_i \qquad (C3)$$

A unit of time is defined as $t = \frac{nc}{U}$, which corresponds to a downstream movement of the vortex sheet of n chords. During this time interval the downwash and sidewash, acting on a line vortex, are assumed constant. The displacements $\Delta y'$ and $\Delta z'$ of a line vortex, induced by the remainder of the vortex system during time t, are then

$$\Delta y' = vt = \frac{ncv}{U}$$

$$\Delta z' = wt = \frac{ncw}{U} \qquad (C4)$$

An implicit assumption of this approximation is that the trailing vortices are generators of semi-infinite cylinders, whereas the vortices actually generate surfaces more nearly resembling cones (reference 7). Successive application of equations (C1), (C3), and (C4), introducing the line vortex coordinates calculated in each previous step, yields the displacements of each line vortex at downstream distances nc, 2nc, 3nc, . . ., successively. The accuracy of the approximation is improved, of course, by assuming smaller values of n.

REFERENCES

1. Mirels, Harold, and Haefeli, Rudolph C.: Line-Vortex Theory for Calculation of Supersonic Downwash. NACA TN 1925, 1949.

2. Lagerstrom, P. A., and Graham, Martha E.: Downwash and Sidewash Induced by Three-Dimensional Lifting Wings in Supersonic Flow. Rep. No. SM-13007, Douglas Aircraft Co., Inc., April 14, 1947.

3. Heaslet, Max A., and Lomax, Harvard: The Calculation of Downwash behind Supersonic Wings with an Application to Triangular Plan Forms. NACA TN 1620, 1948.

4. Perkins, Edward N., and Canning, Thomas N.: Investigation of Downwash and Wake Characteristics at a Mach Number of 1.53. I - Rectangular Wing. NACA RM A8L16, 1949.

5. Adamson, D., and Boatright, William B.: Investigation of Downwash, Sidewash, and Mach Number Distribution behind a Rectangular Wing at a Mach Number of 2.41. NACA RM L50G12, 1950.

6. Spreiter, John R., and Sacks, Alvin H.: The Rolling up of the Trailing Vortex Sheet and Its Effect on the Downwash behind Wings. IAS Preprint 250, Jan., 1950.

7. Cummings, John L., Mirels, Harold, and Baughman, L. E.: Downwash in Vortex Region behind Trapezoidal-Wing Tip at Mach Number 1.91. NACA RM E9H15, 1949.

8. Westwater, F. L.: Rolling Up of the Surface of Discontinuity behind an Airfoil of Finite Span. R. & M. No. 1692, British A.R.C., Aug. 1935.

9. Haefeli, Rudolph C., Mirels, Harold, and Cummings, John L.: Charts for Estimating Downwash behind Rectangular, Trapezoidal, and Triangular Wings at Supersonic Speeds. NACA TN 2141, 1950.

10. Silverstein, Abe, Katzoff, S., and Bullivant, W. Kenneth: Downwash and Wake behind Plain and Flapped Airfoils. NACA Rep. 651, 1939.

TABLE I. - COORDINATES OF SPANWISE STATIONS

Station	y		
	Downwash survey		Wake pressure survey
	x = 1.5	x = 3	
a	1.25	1.25	
b	1.14	1.13	
c	1.02	1.01	
d	.90	.89	
e	.78	.77	
f	.66	.65	
g	.54	.53	
h	.42	.42	
i	.30	.30	
j	.18	.18	
k	.07	.06	
l	- .05	- .06	-0.08
m		- .18	- .20
n	- .29	- .30	- .32
o		- .42	- .44
p	- .53	- .53	
q		- .65	
r	- .77	- .77	- .79
s		- .89	
t		-1.13	-1.15
u			-1.27
v		-1.37	
w		-1.61	
x		-1.85	

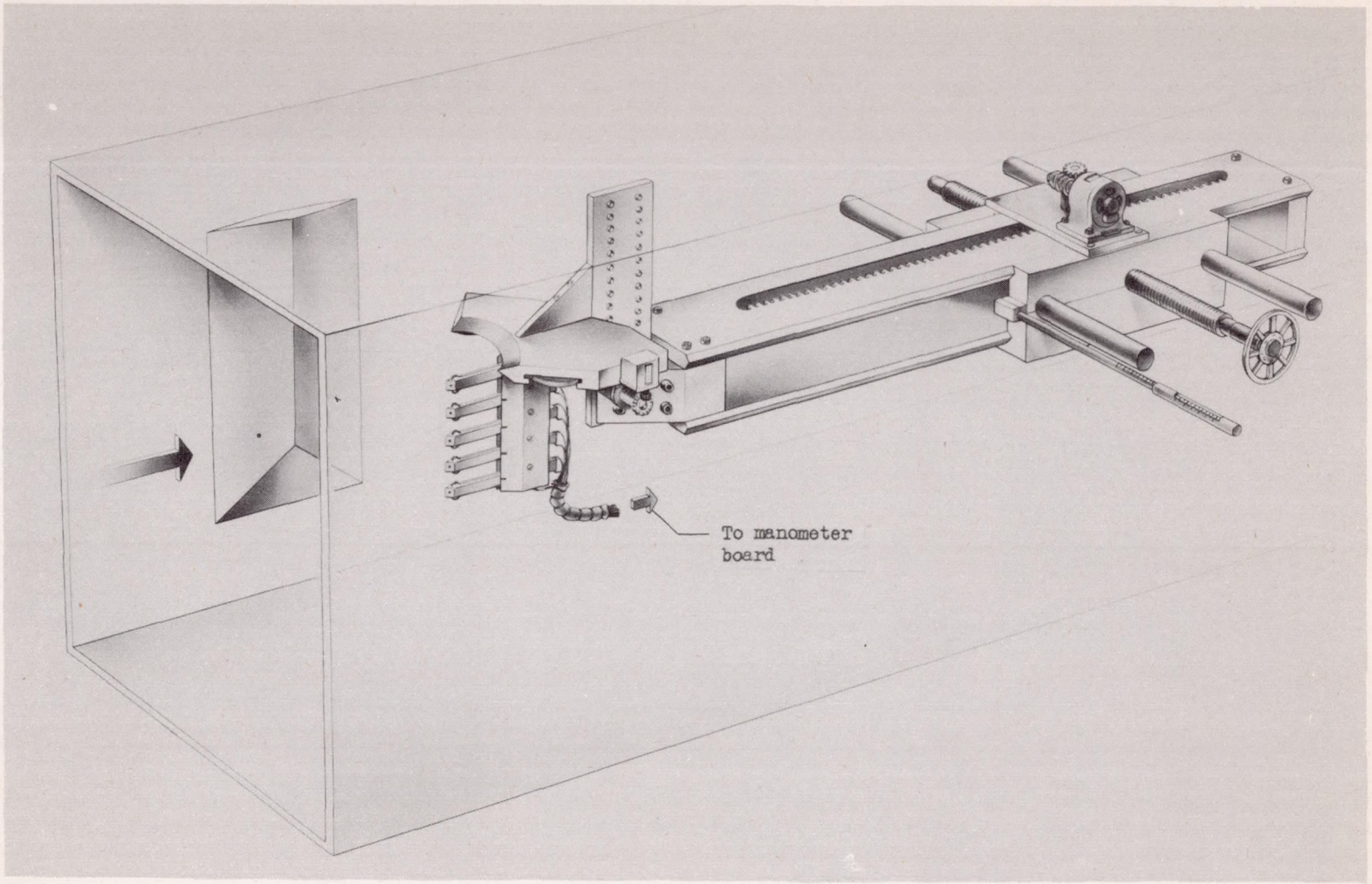

Figure 1. - Rectangular wing and apparatus for measuring downwash as mounted in tunnel.

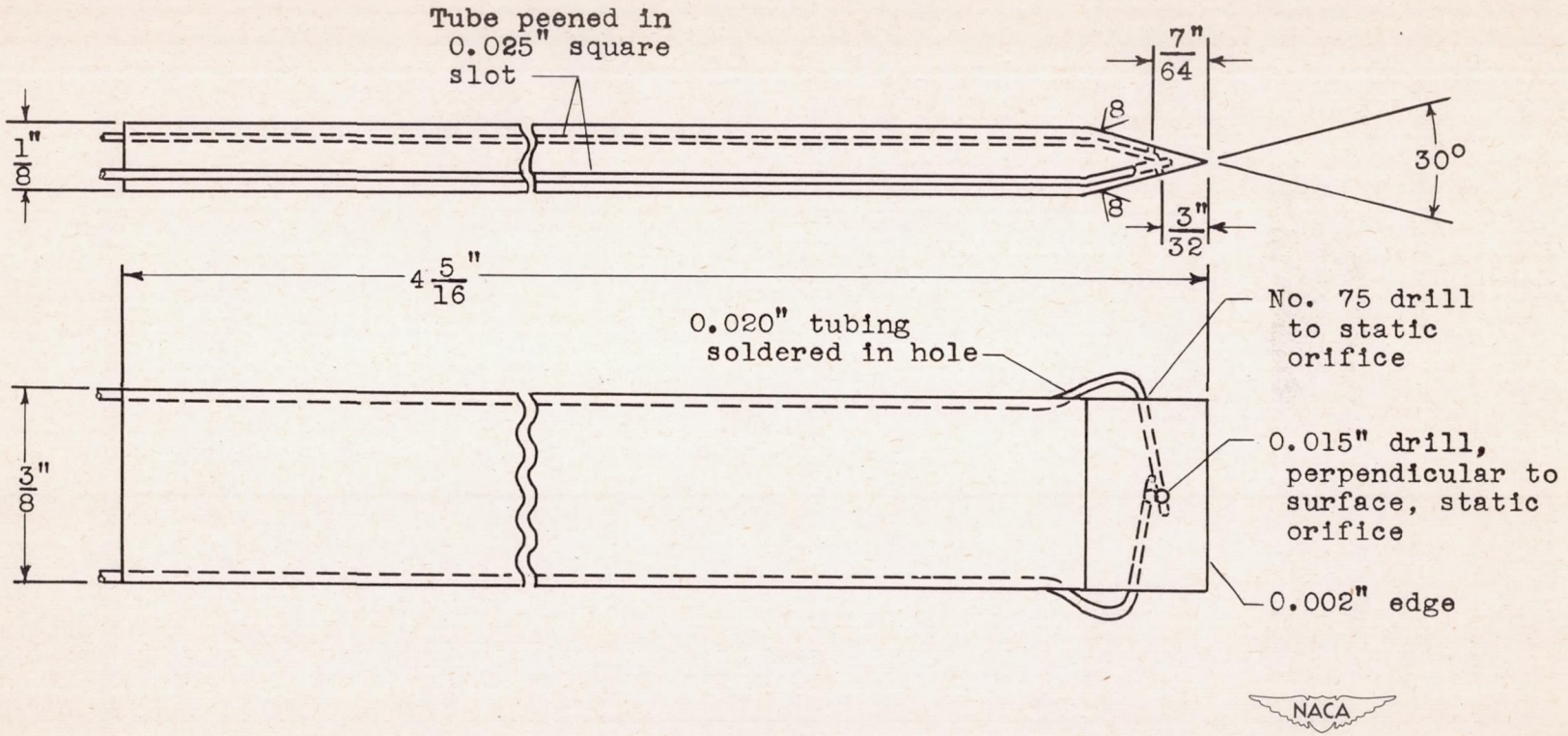

Figure 2. - Wedge used for measuring downwash.

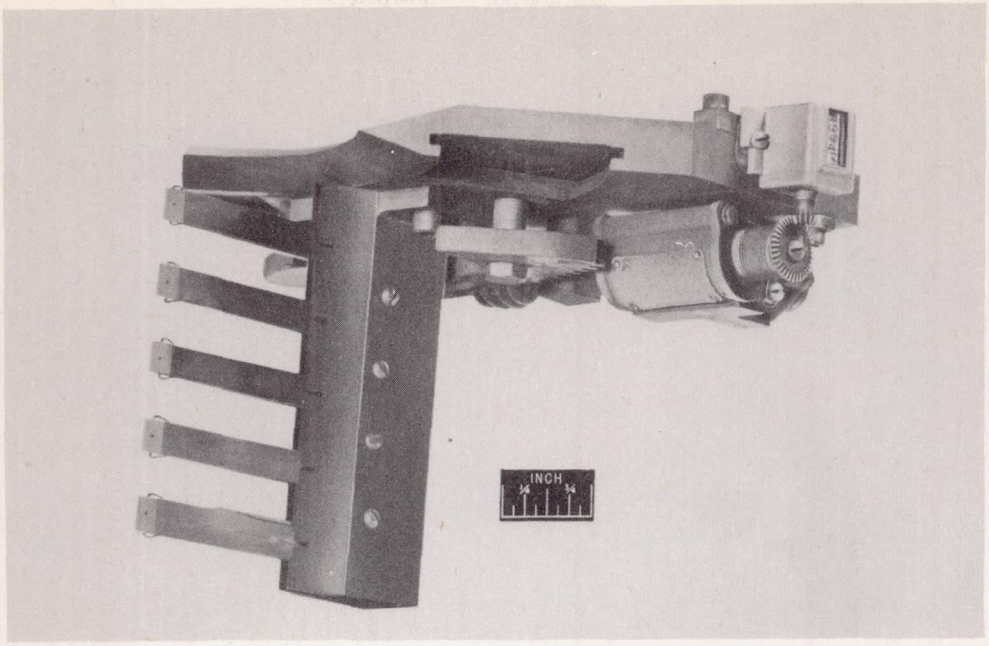

(a) Wedge mechanism.

NACA
C-24663

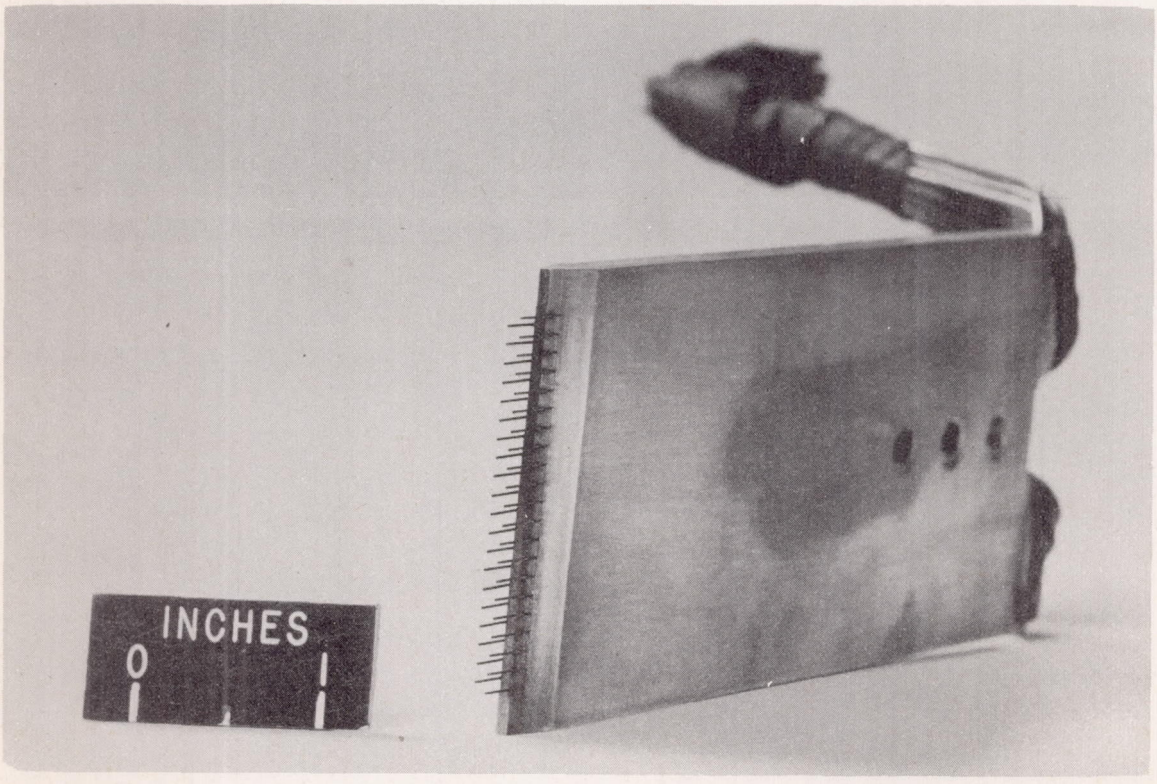

(b) Wake-survey rake.

NACA
C-23131

Figure 3. - Apparatus used in investigation.

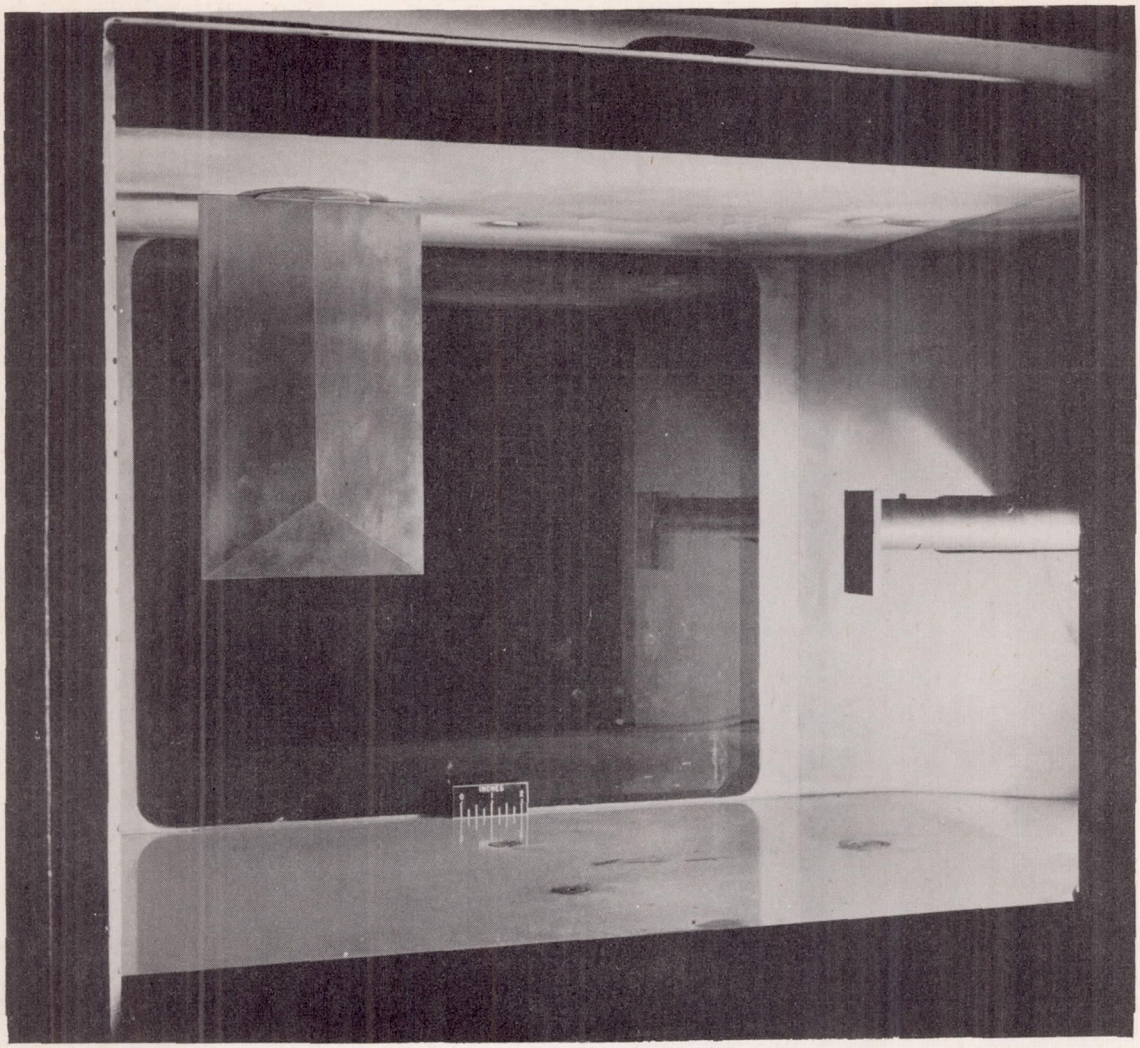

(c) Flat plate installed downstream of wing in tunnel. NACA C-25262

Figure 3. - Concluded. Apparatus used in investigation.

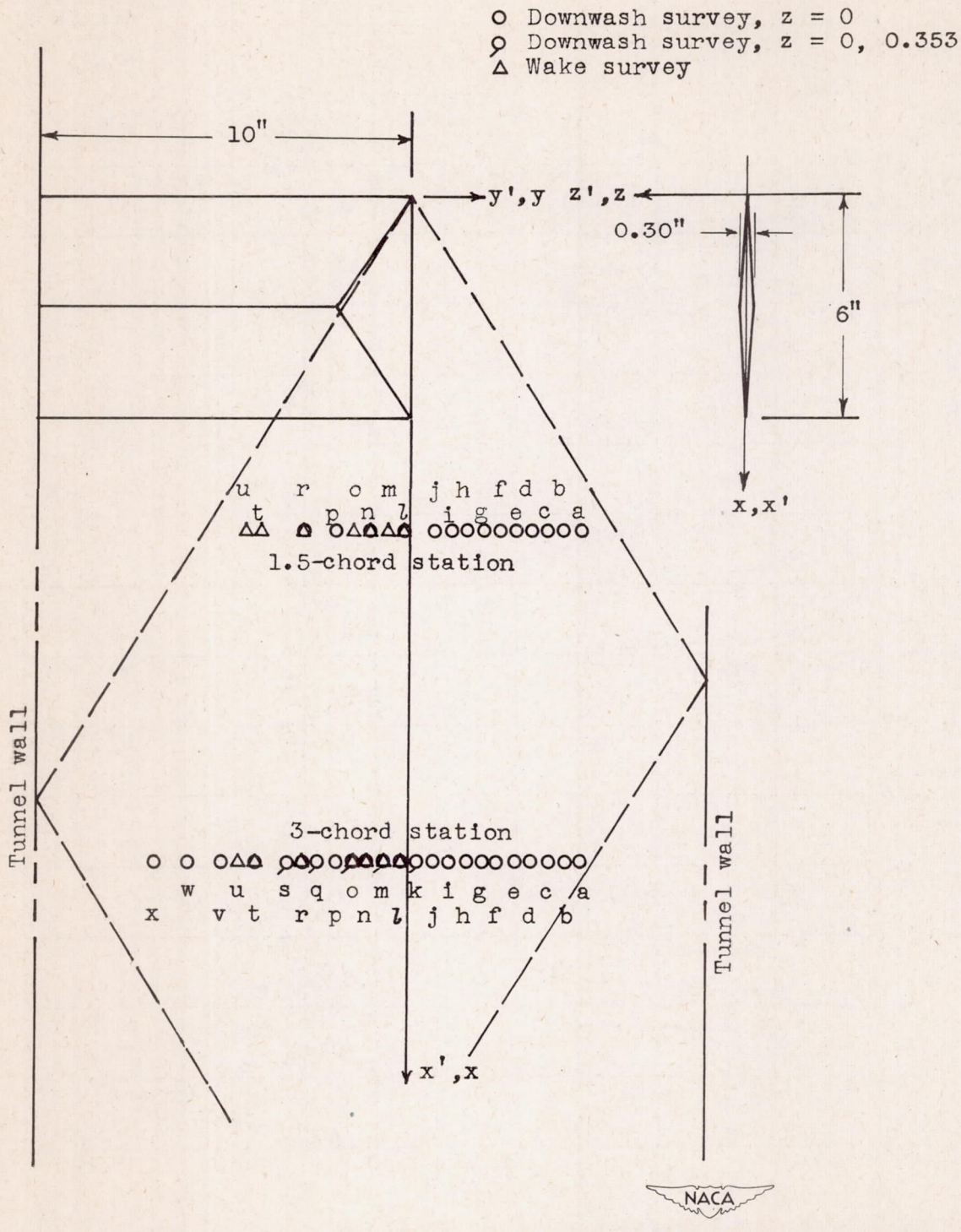

Figure 4. - Rectangular wing and survey stations.

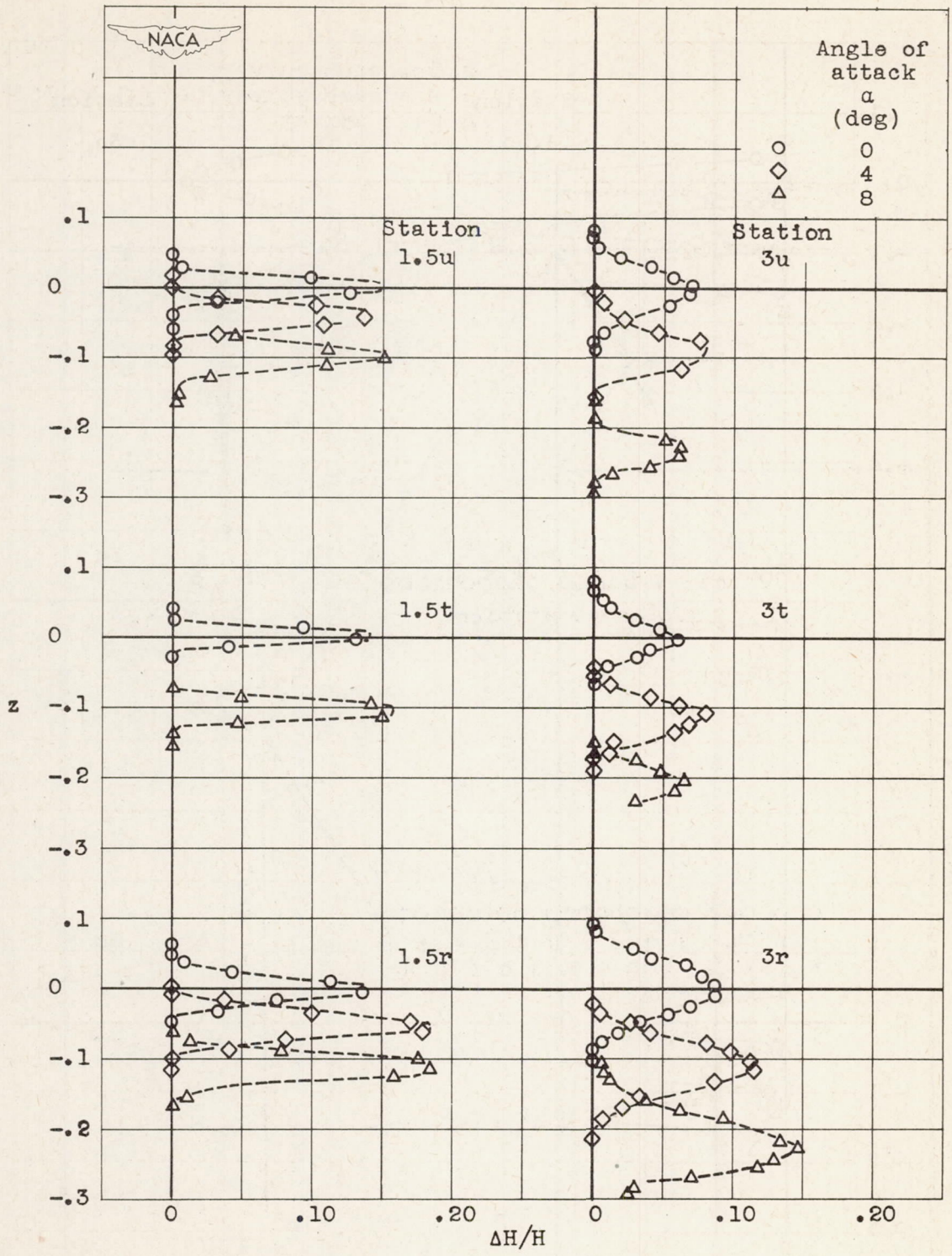

(a) Stations u, t, and r.

Figure 5. - Profiles of wake intensity behind rectangular wing. x = 1.5 and 3.

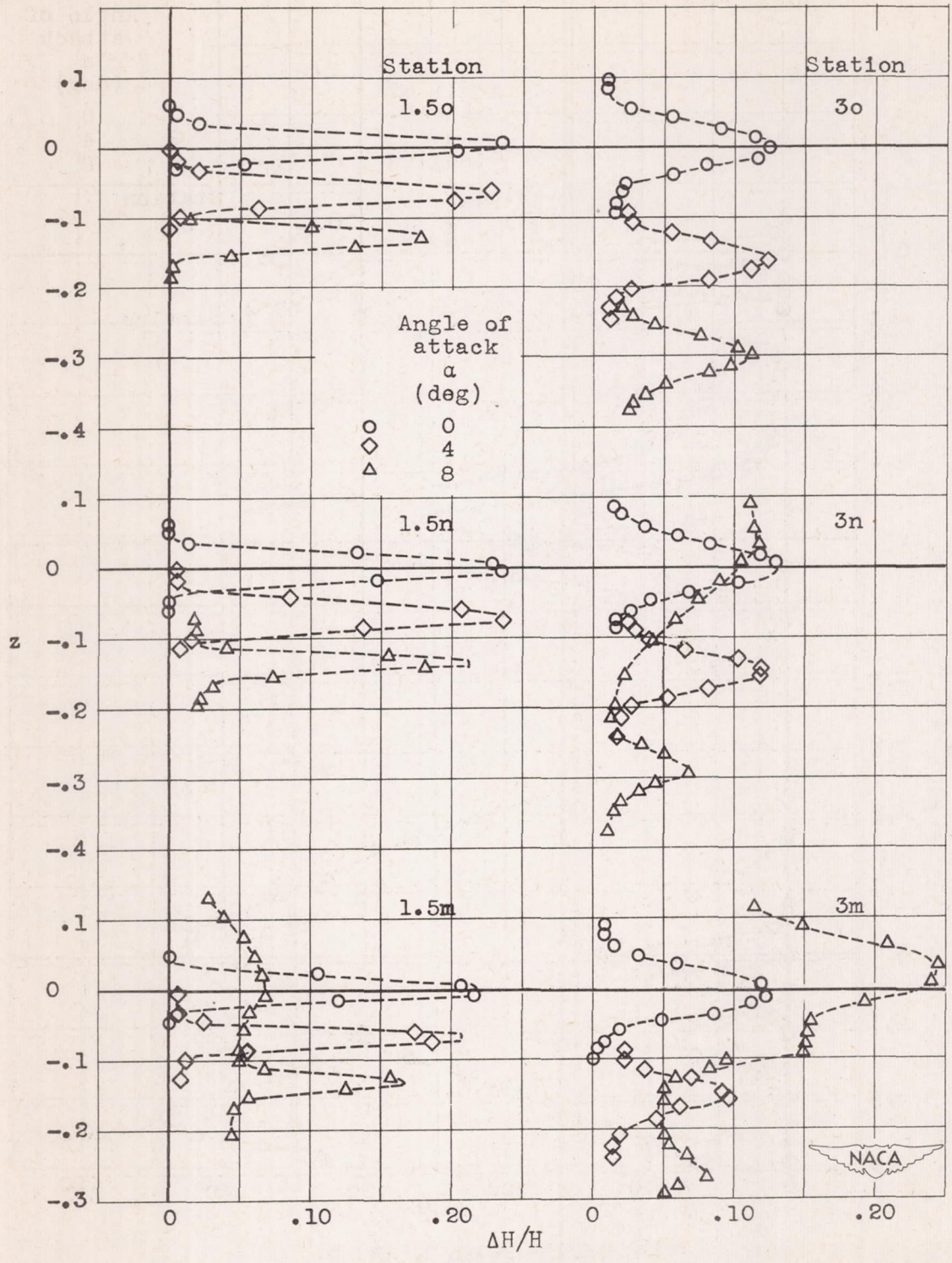

(b) Stations o, n, and m.

Figure 5. - Continued. Profiles of wake intensity behind rectangular wing. x = 1.5 and 3.

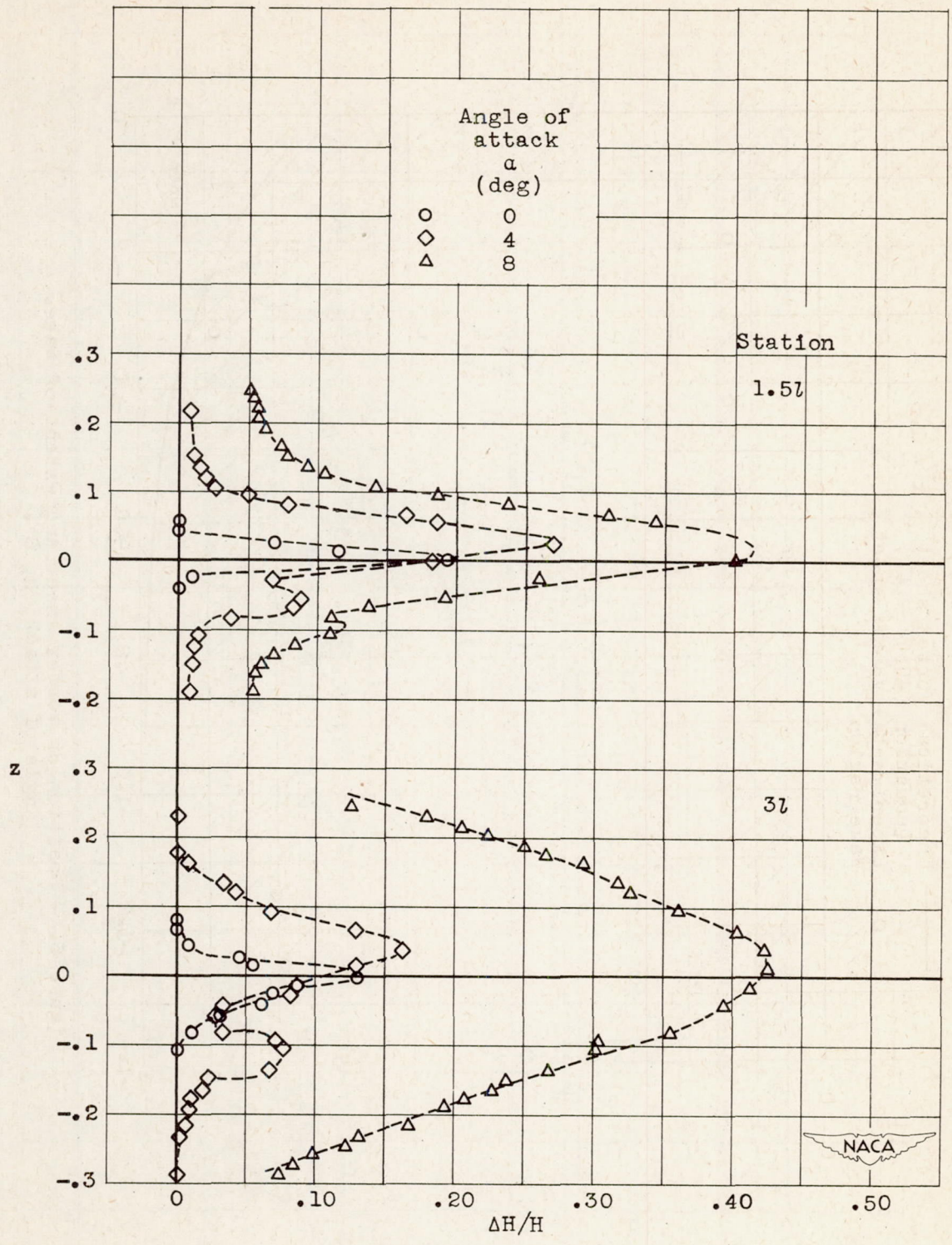

(c) Station l.

Figure 5. - Concluded. Profiles of wake intensity behind rectangular wing. x = 1.5 and 3.

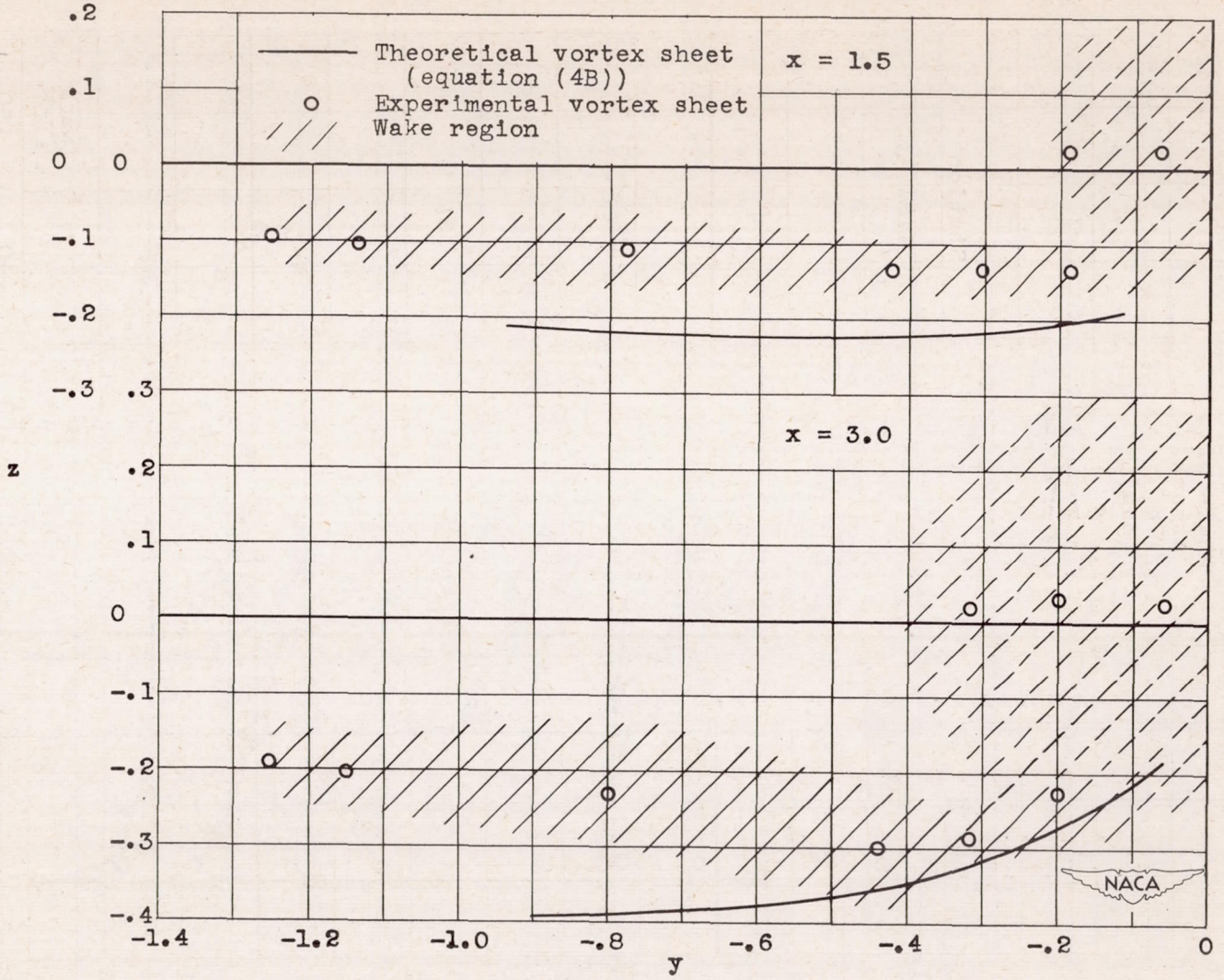

Figure 6. - Position of vortex sheet and extent of wake.
Angle of attack, α, 8°.

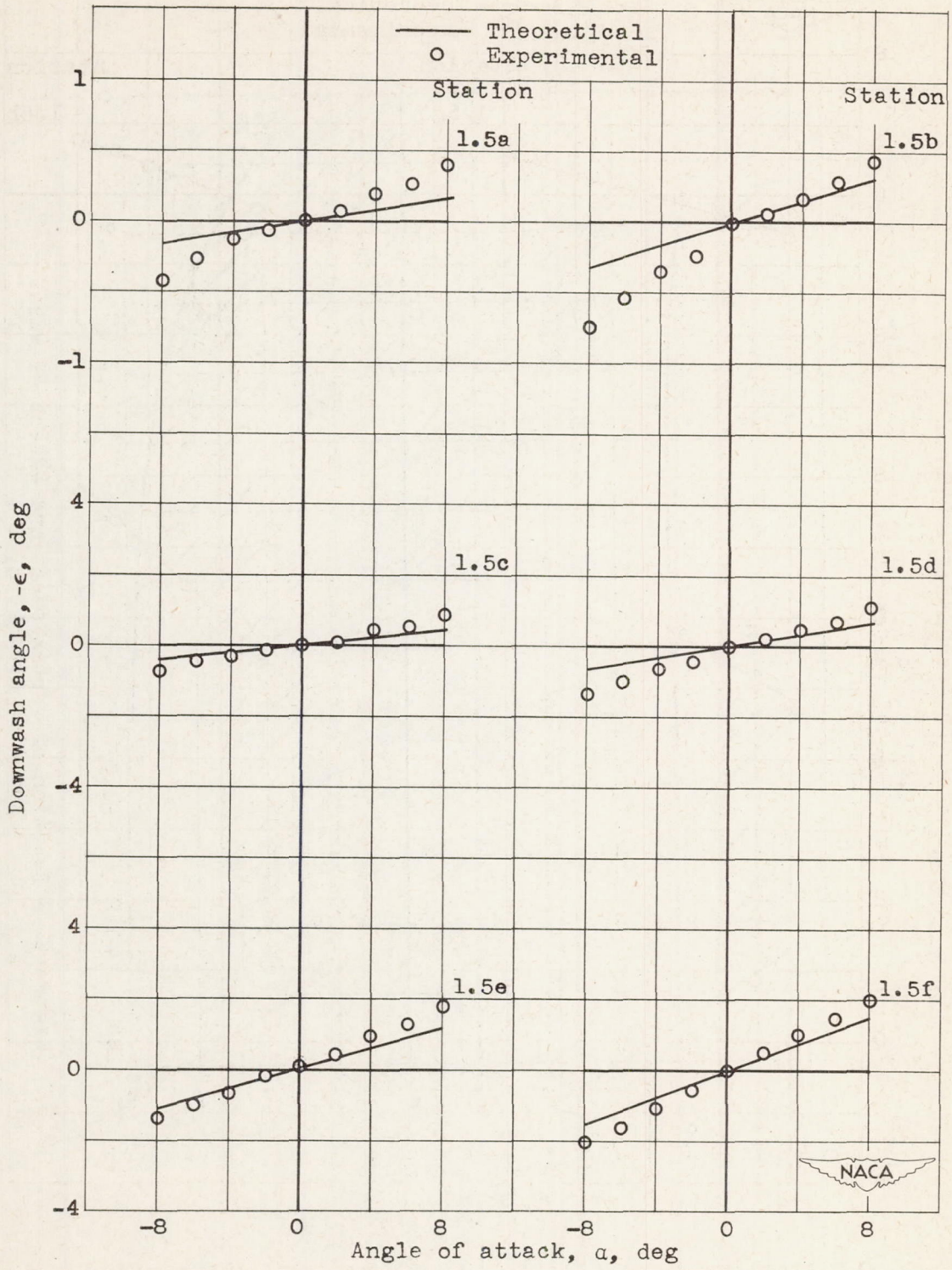

(a) Stations 1.5a to 1.5f; x = 1.5; z = 0.

Figure 7. - Variation of downwash angle with angle of attack.

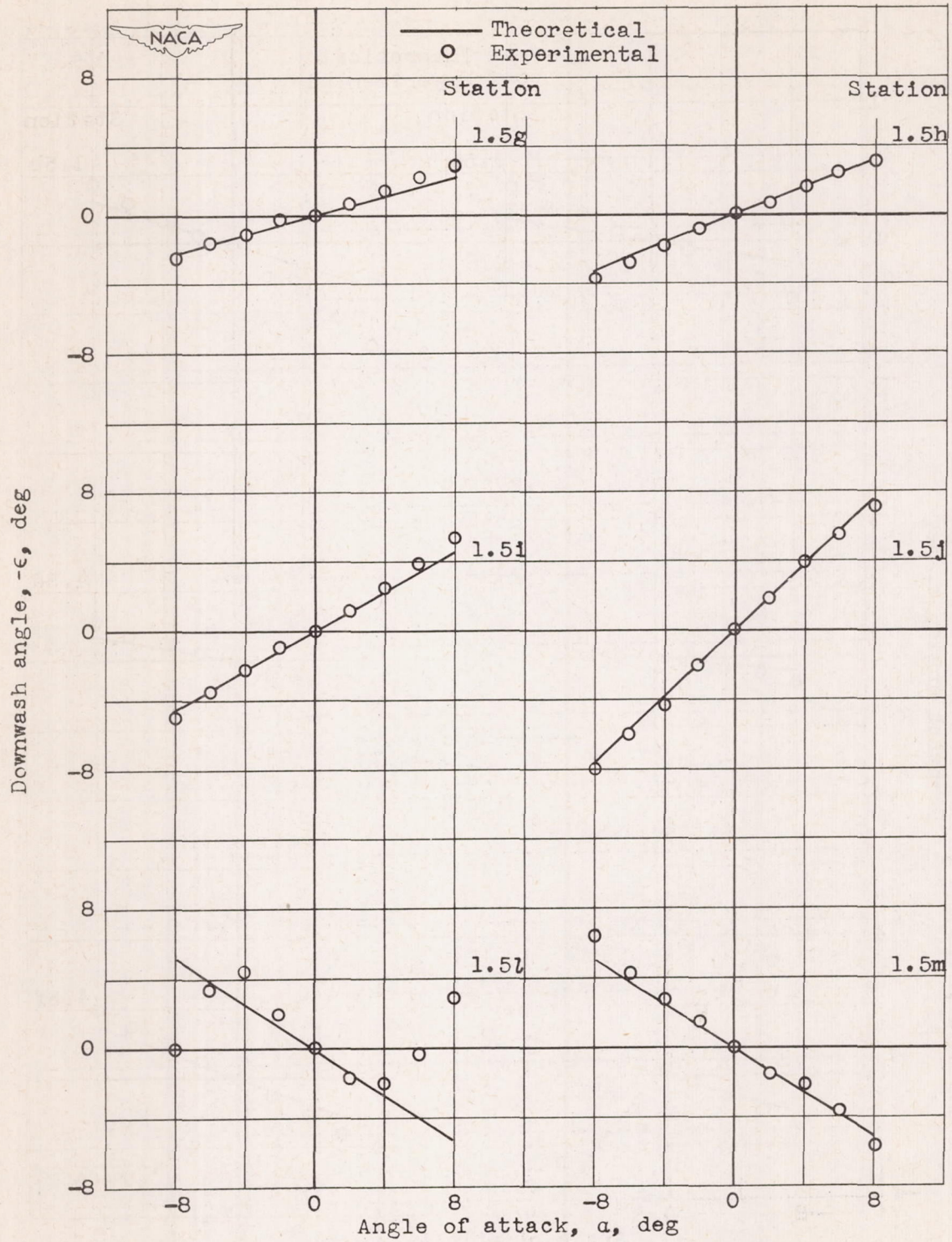

(b) Stations 1.5g to 1.5j, 1.5l, 1.5m; x = 1.5; z = 0.

Figure 7. - Continued. Variation of downwash angle with angle of attack.

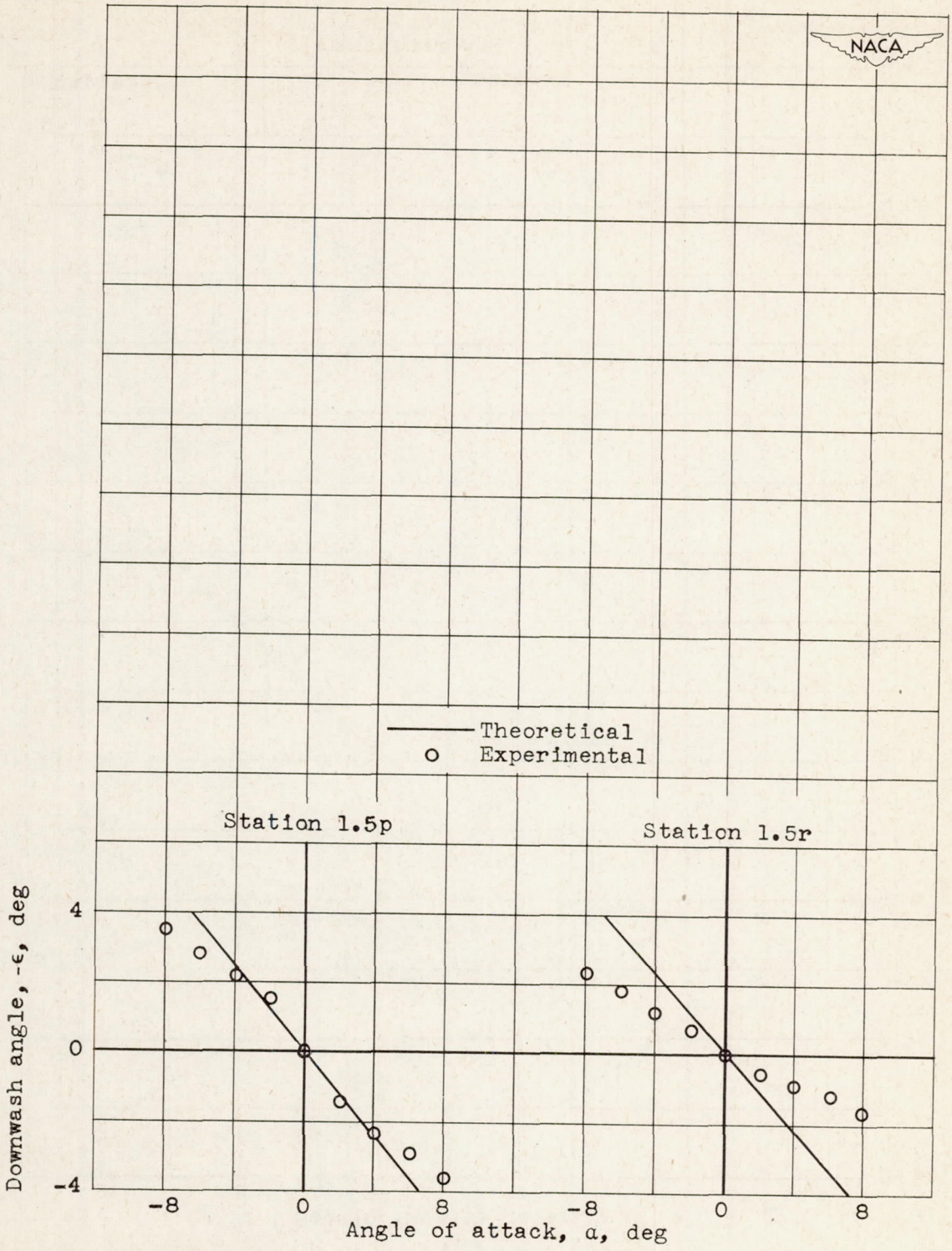

(c) Stations 1.5p and 1.5r; x = 1.5; z = 0.

Figure 7. - Continued. Variation of downwash angle with angle of attack.

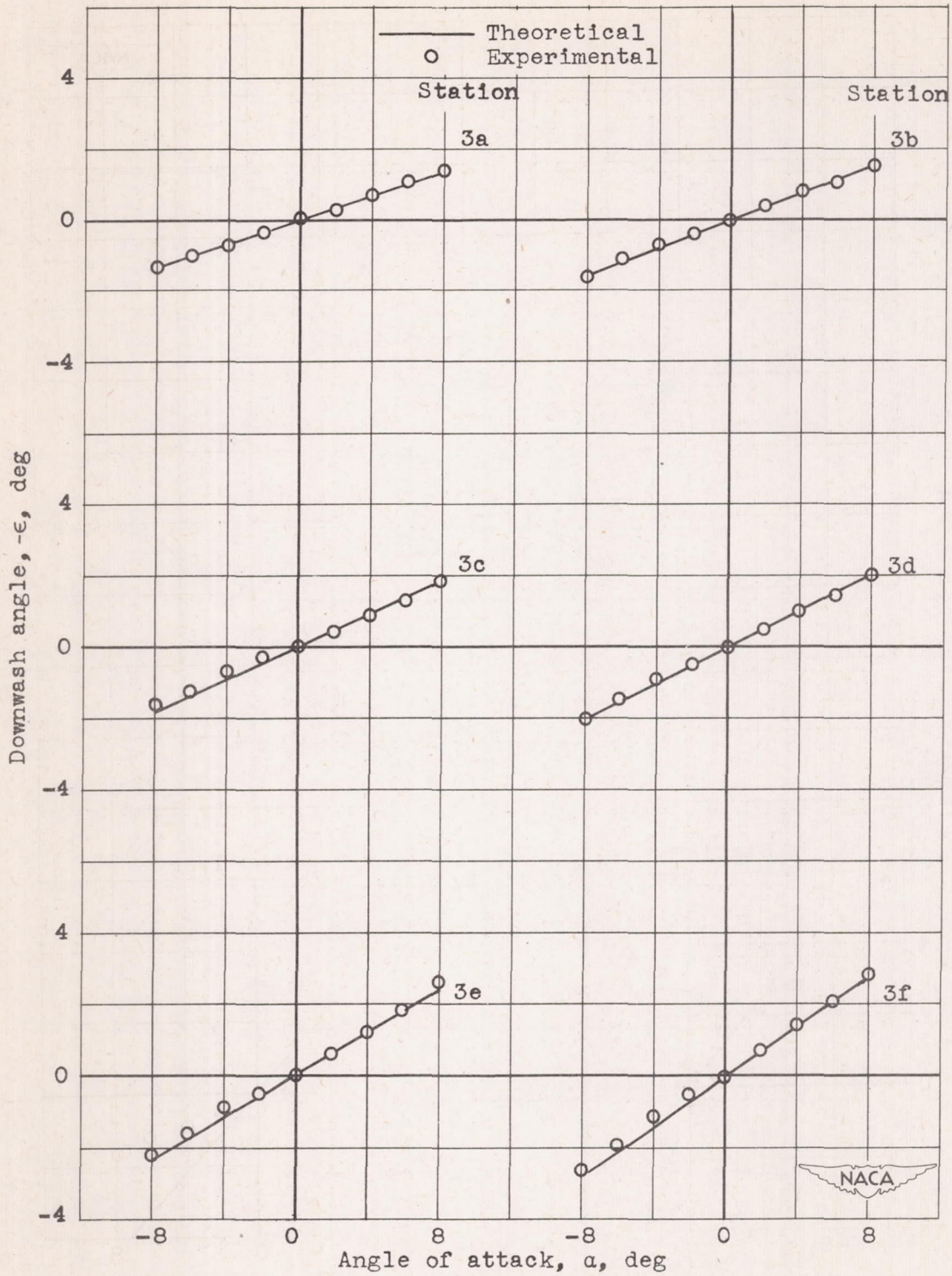

(d) Stations 3a to 3f; x = 3; z = 0.

Figure 7. - Continued. Variation of downwash angle with angle of attack.

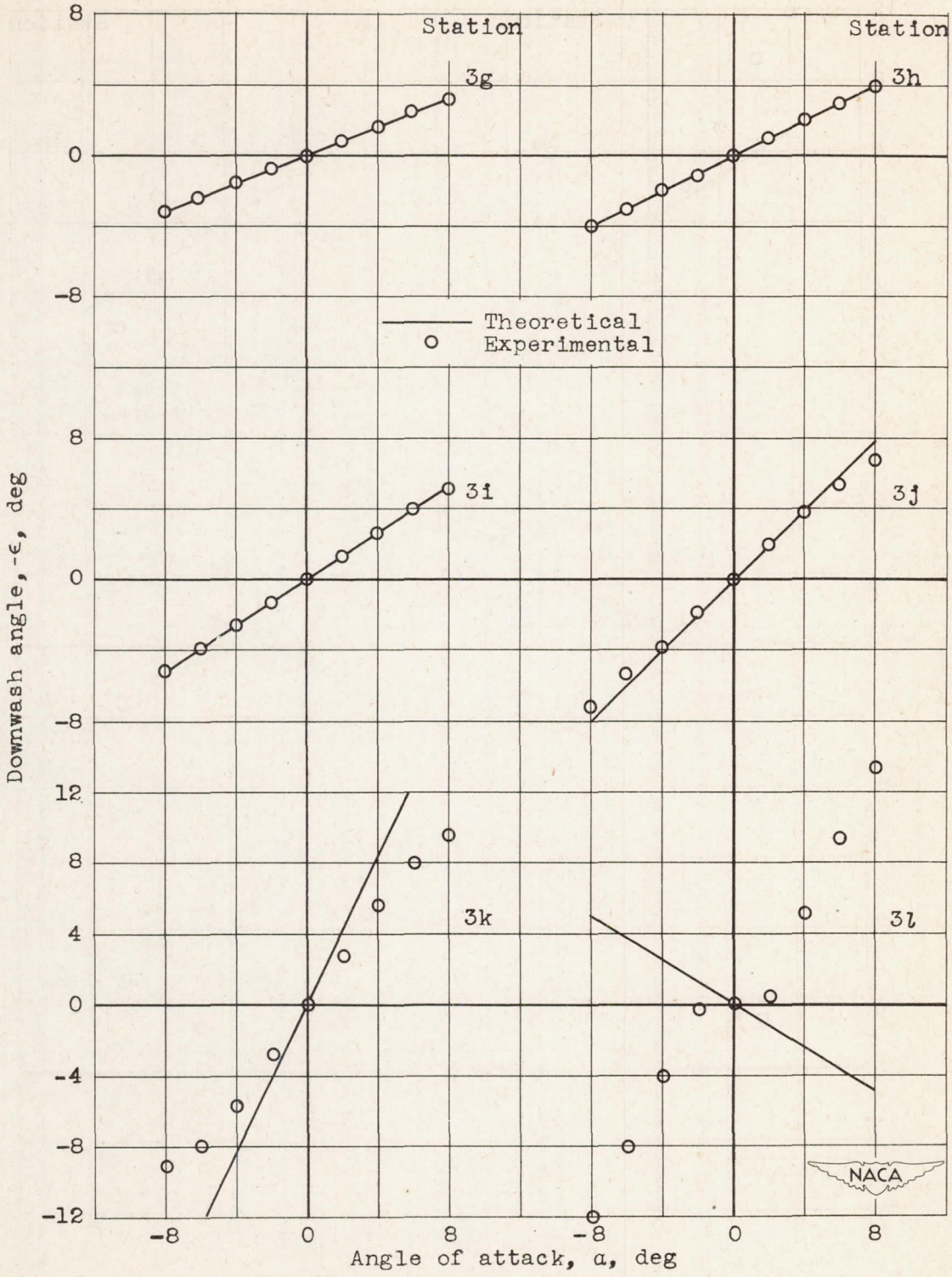

(e) Stations 3g to 3l; x = 3; z = 0.

Figure 7. - Continued. Variation of downwash angle with angle of attack.

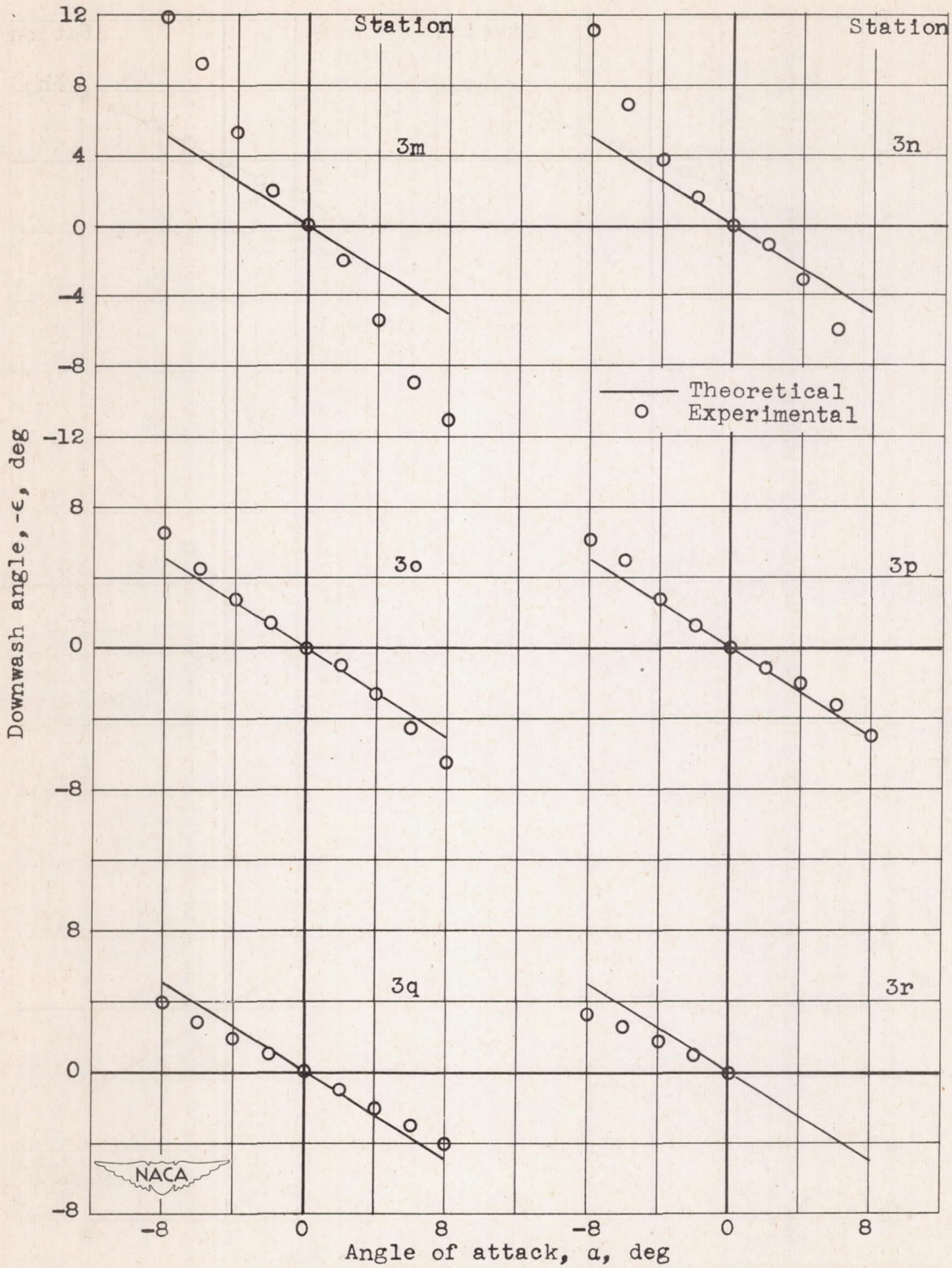

(f) Stations 3m to 3r; x = 3; z = 0.

Figure 7. - Continued. Variation of downwash angle with angle of attack.

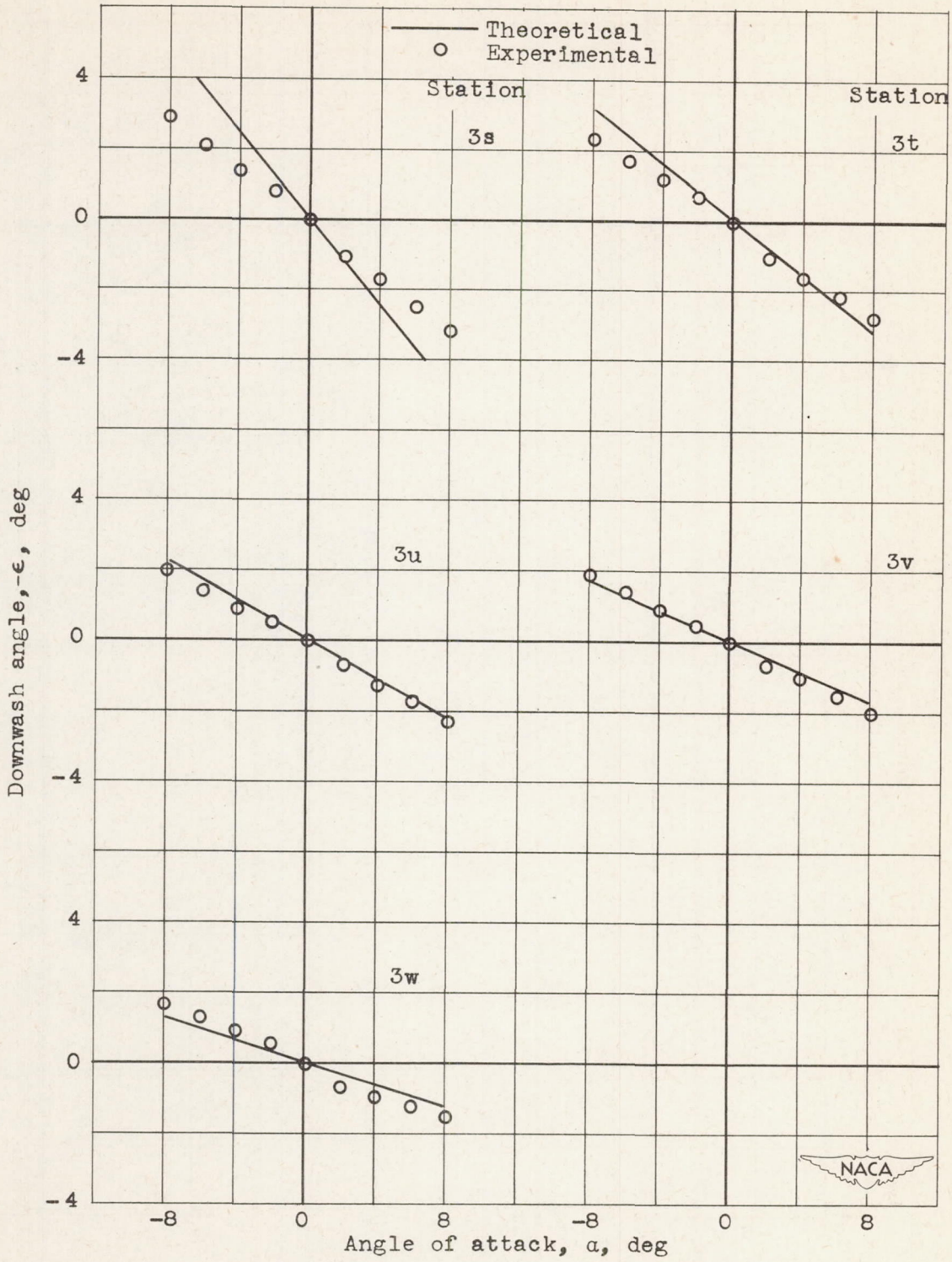

(g) Stations 3s to 3w; x = 3; z = 0.

Figure 7. - Continued. Variation of downwash angle with angle of attack.

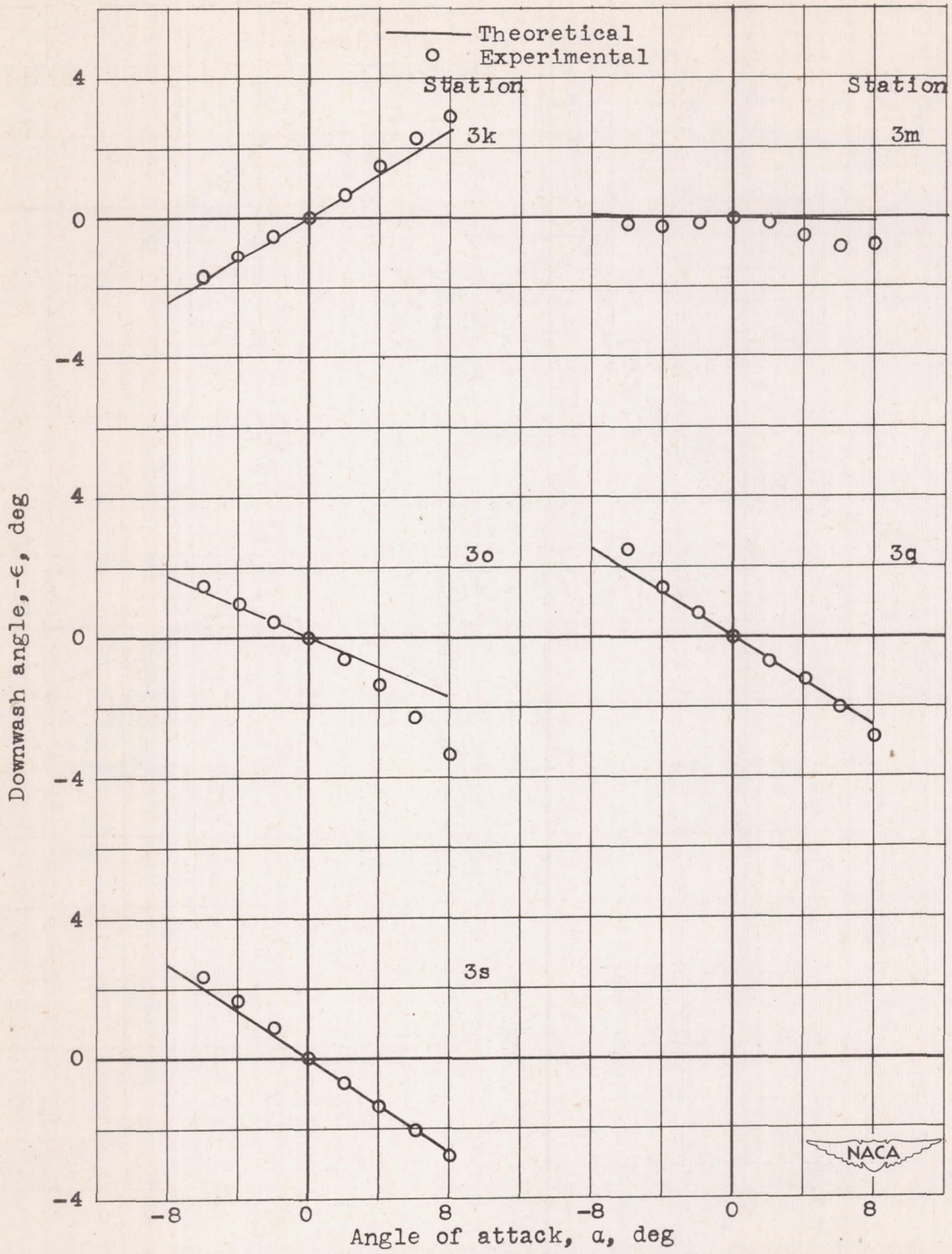

(h) Stations 3k, 3m, 3o, 3q, 3s; x = 3; z = 0.353.

Figure 7. - Concluded. Variation of downwash angle with angle of attack.

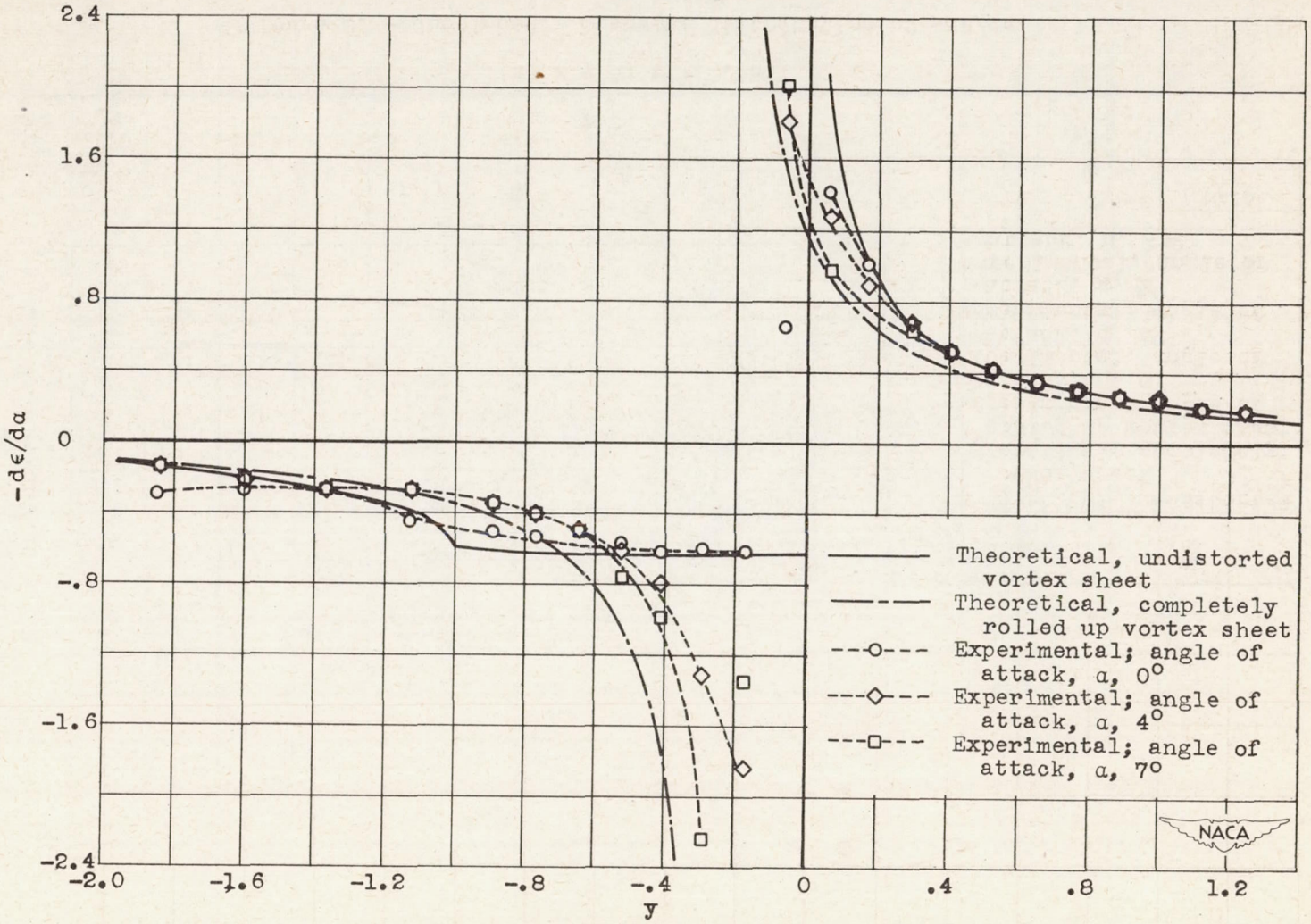

(a) x = 3; z = 0.

Figure 8. - Spanwise distribution of $-d\epsilon/d\alpha$.

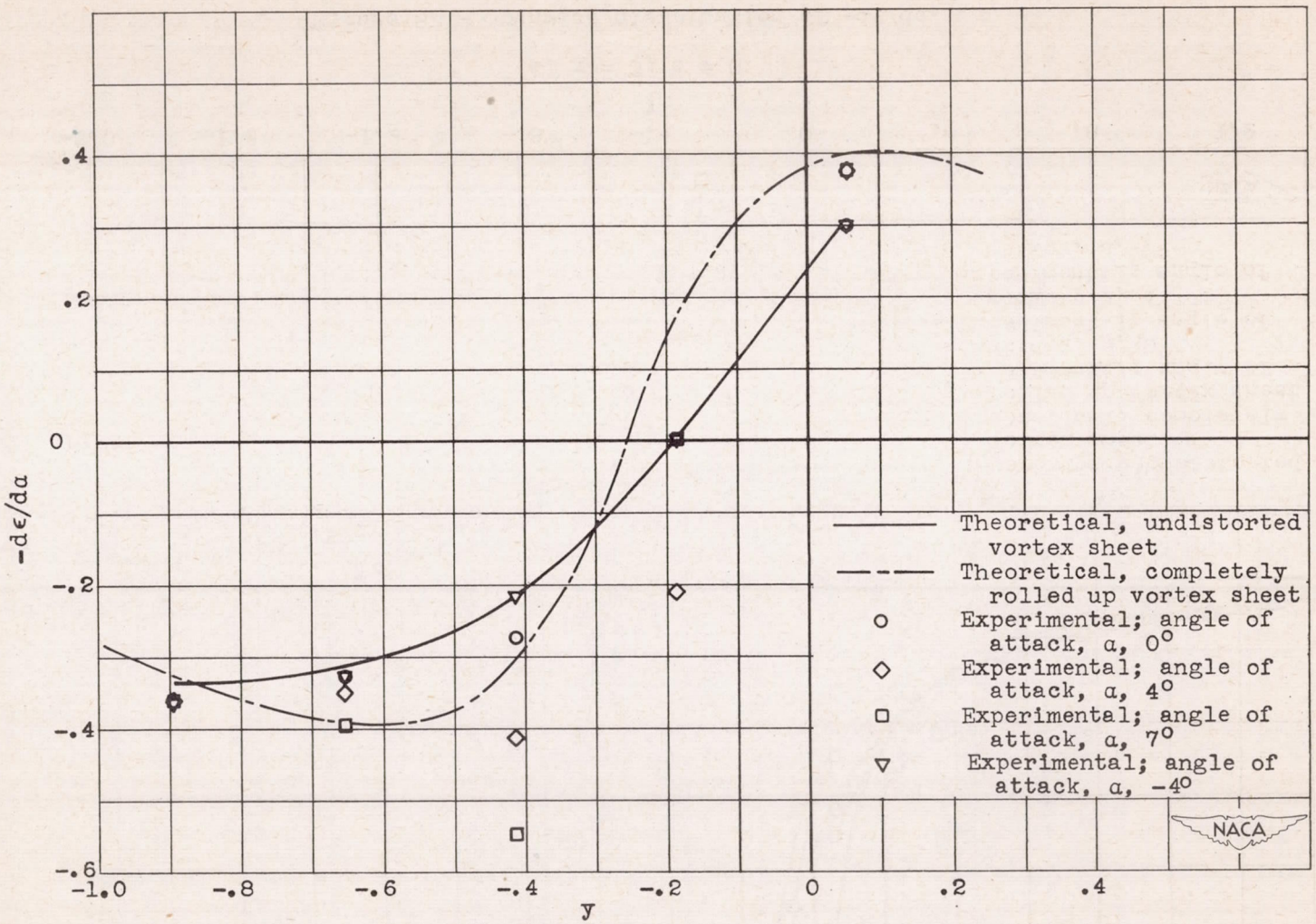

(b) x = 3; z = 0.353.

Figure 8. - Continued. Spanwise distribution of -dε/dα.

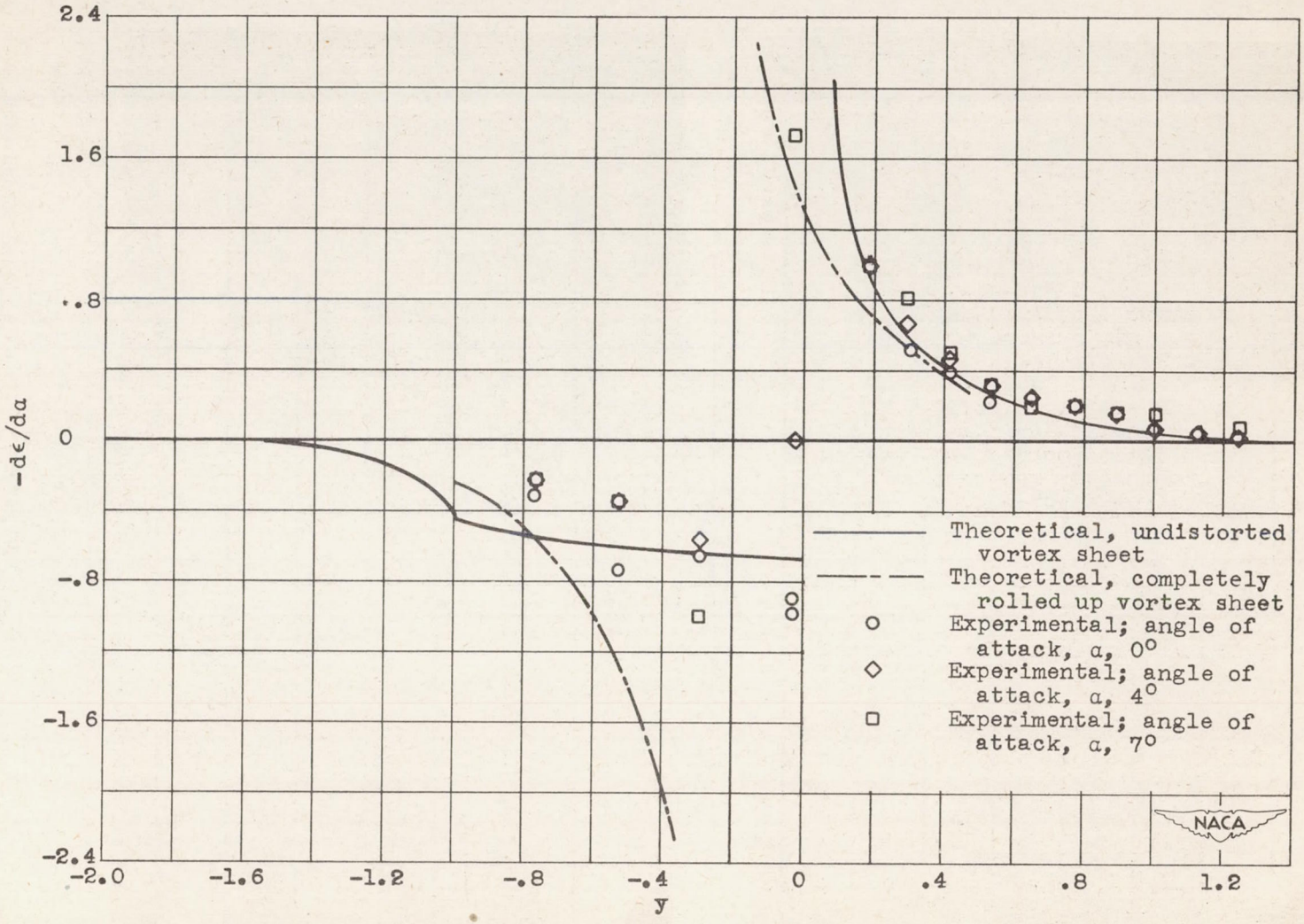

(c) x = 1.5; z = 0.

Figure 8. - Concluded. Spanwise distribution of $-d\epsilon/d\alpha$.

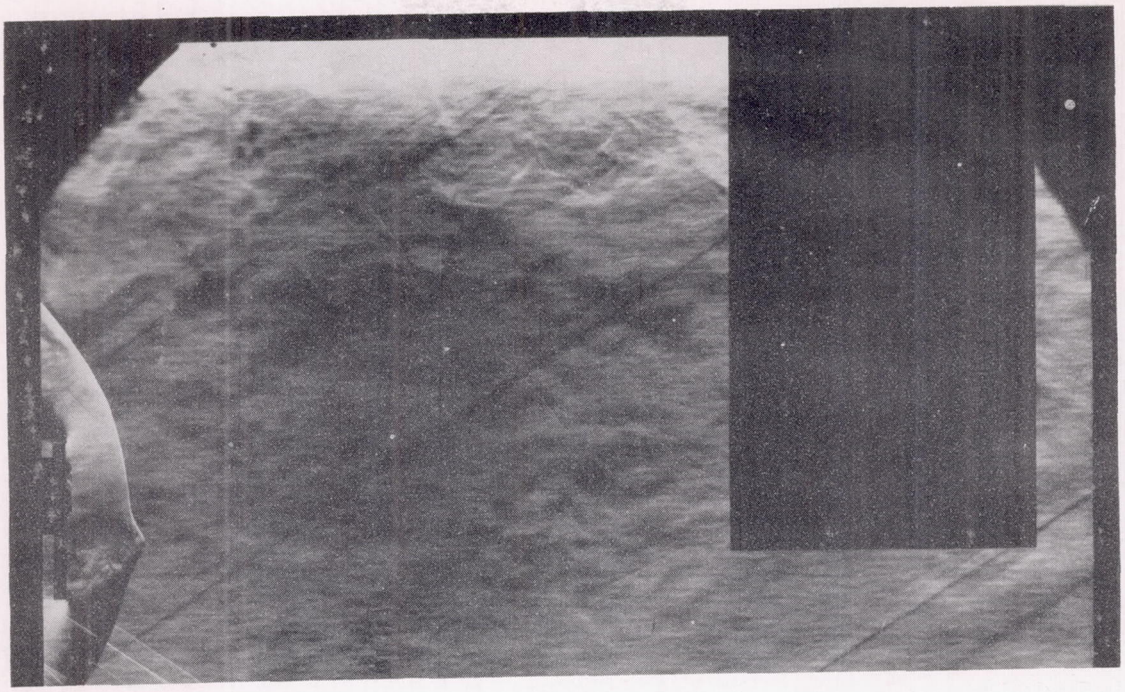

(a) Angle of attack, α, -2°.

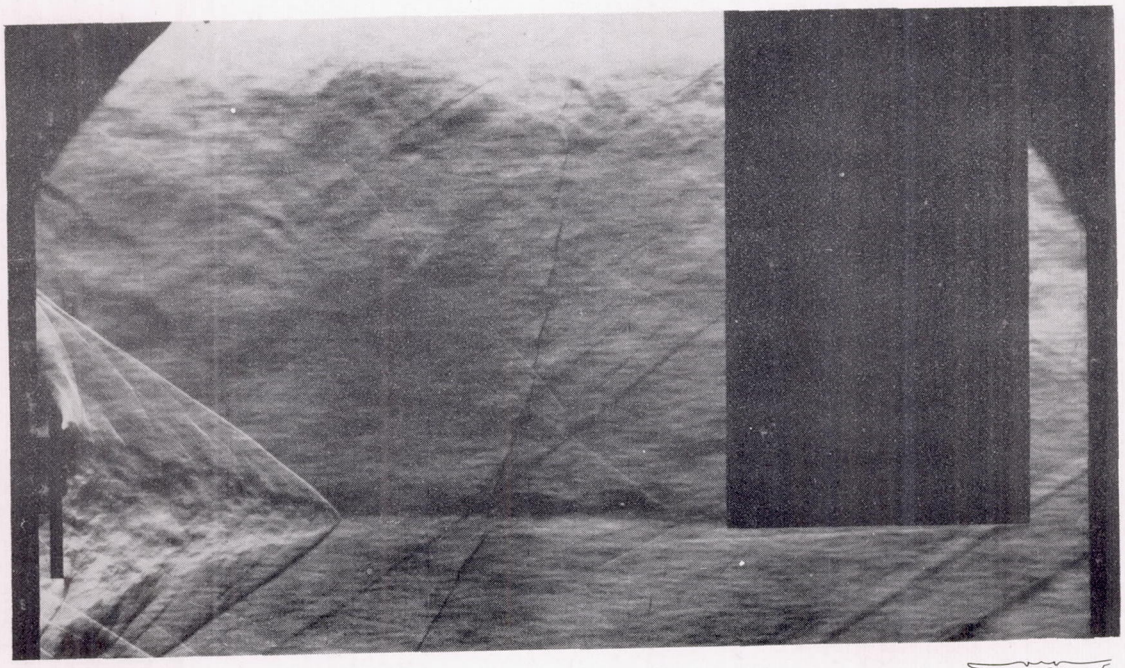

NACA

C-26374

(b) Angle of attack, α, -8°.

Figure 9. - Flash schlieren photographs with flat plate installed behind wing.

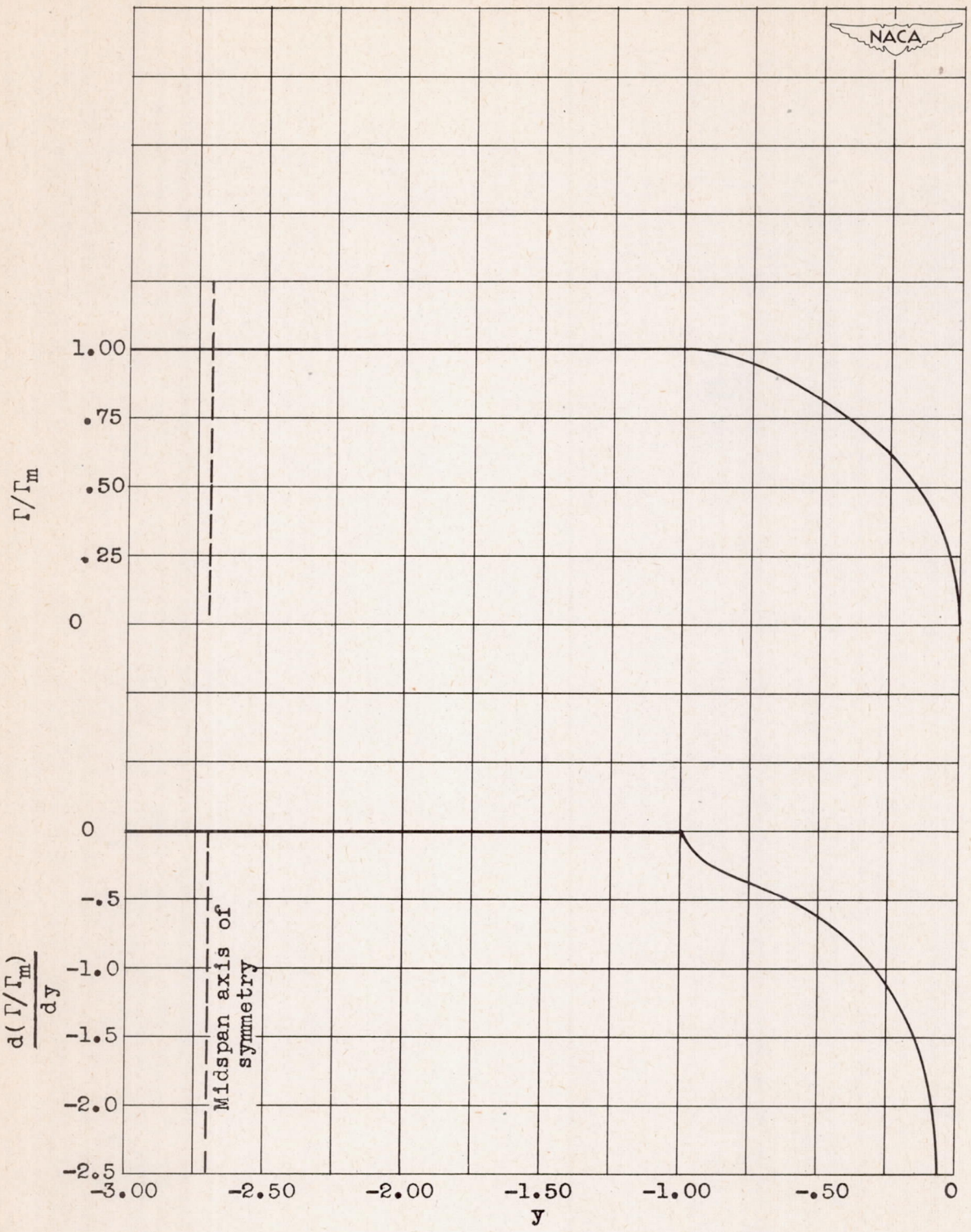

Figure 10. - Spanwise distribution of circulation Γ/Γ_m and shed vorticity $\frac{d(\Gamma/\Gamma_m)}{dy}$ for rectangular wing. $\frac{\Gamma_m}{aVc} = 1.23$.

NACA-Langley - 10-26-50 - 350